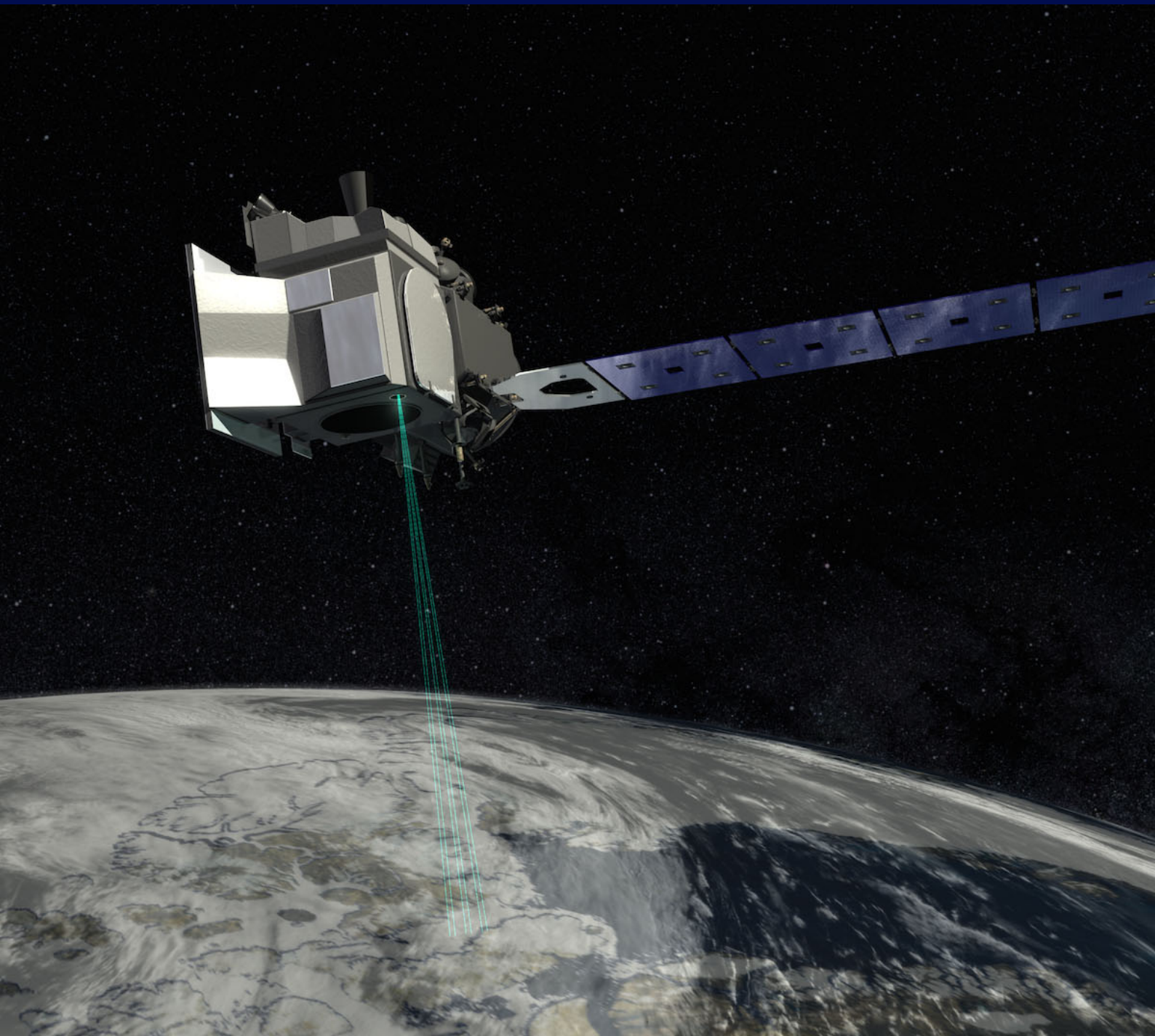


Bathymetric mapping Using ICESat-2 LIDAR and Sentinel-2 multi- spectral imagery

Master Thesis



Bathymetric mapping

Using ICESat-2 LIDAR and Sentinel-2 multi-spectral imagery

Master Thesis

January, 2021

Author:

Pernille Kliving

Supervisors:

Ole Baltazar Andersen

&

Heidi Ranndal

Approval

Pernille Kliving - s151722

Pernille Kliving

.....
Signature

20/1/2021

.....
Date

Abstract

There is a need for near-shore bathymetric mapping for ship navigation and monitoring effects of climate change and natural disasters. This project presents the benefits and limitations of boat and airborne methods, which often have high accuracy but are time consuming and expensive. Therefore satellite based methods have become increasingly popular. A method for estimating bathymetry from ICESat-2 LIDAR will be presented in this report. The seafloor photon data is extracted and corrected for refraction and tides. The results are validated using single beam echo sounding data. ICESat-2 bathymetry shows promise, as it is able to estimate bathymetry with an accuracy resulting in a RMSE of 1.5-3.5 % of the maximum depth. However, there are limitations to ICESat-2 LIDAR bathymetry, ones being the spatial coverage which is limited to tracks. Since surface coverage is often needed, a satellite derived bathymetry method using multi-spectral images from Sentinel-2 combined with the ICESat-2 estimated depths is proposed. For most methods deriving bathymetry from multi-spectral imaging, in situ measurements are essential. By using ICESat-2 in place of in situ measurements, it is possible to create a method based solely on satellite data. The combined Sentinel-2 and ICESat-2 data is used in a linear band model and implemented using least square regression. The resulting model had an RMSE accuracy of 0.79-9.2 % of the maximum depth.

Acknowledgements

I would like to thank my supervisors Ole Baltazar Andersen and Heidi Ranndal from DTU Space for patience, encouragements and support throughout this project. Thank you for challenging me along the way, so that the project would be as good as possible.

This project would not have been possible without the help of Laurids Rolighed Larsen, Peter Gelsbo and Klavs Bundgaard from *NIRAS*. Thank you for all the time and effort you put into this project. It has been very helpful to have your insight and comments throughout the last 6 months. The provided data sets and knowledge of the study area has been very valuable and appreciated.

A big thank you is also owed to Mikkel Lydholm Rasmussen and Lisbeth Tangaa Nielsen from DHI GRAS for sharing information and knowledge of satellite derived bathymetry.

Finally thank you to all my amazing friends at DTU Space, who were always up for discussing ideas and challenges over lunch.

Contents

Preface	ii
Abstract	iii
Acknowledgements	iv
1 Introduction	1
1.1 Motivation	1
1.2 Satellite based methods for bathymetric mapping	1
1.3 Project goals	2
2 Bathymetric Mapping	4
2.1 LIDAR Bathymetry	5
2.1.1 Refraction	6
2.2 Satellite Derived Bathymetry using multi-spectral images	9
2.2.1 Linear Band Model for estimating bathymetry	10
2.2.2 Implementation of Linear Band Model	11
2.3 Echo Sounders	13
3 Study Area and Data	15
3.1 Study Area	15
3.2 Data	17
3.2.1 ICESat-2	17
3.2.2 Sentinel-2	21
3.2.3 Single Beam Echo Sounding	23
3.2.4 Mean Sea Level data	24
4 Methods and Data processing	25
4.1 ICESat-2 LIDAR	25
4.1.1 Separate seafloor and water surface	25
4.1.2 Define water surface	26
4.1.3 Tidal and Refraction correction	27
4.1.4 Outlier removal and smoothing	28
4.2 Sentinel-2 multi-spectral imagery	31
4.2.1 Resample images	32
4.2.2 Subset Images	32
4.2.3 Land and cloud mask	32
4.2.4 Sun-glint	33
4.3 Combining ICESat-2 and Sentinel-2 for satellite derived bathymetry	35

5 Results	36
5.1 ICESat-2 LIDAR Bathymetry	36
5.1.1 Visual Inspection of ICESat-2 bathymetry	39
5.2 Combined Sentinel-2 & ICESat-2 Satellite Derived Bathymetry . .	44
5.2.1 Optimizing Satellite Derived Bathymetry Model	44
5.2.2 Validating final Satellite Derived Bathymetry model	47
5.2.3 Single Beam as input in Linear Band Model	53
6 Conclusion	57
7 Future Work	60
Bibliography	62

1 Introduction

1.1 Motivation

Bathymetry is the information of underwater topography and water depths. The ocean covers more than 70% of the Earth's surface, yet only a small part has been mapped directly. With climate change, natural disasters, habitat loss and an increase in offshore energy amongst other things, there is a growing need for bathymetric mapping (Wöfl et al., 2019). The need for assessing climate change impact in coastal environments makes near-shore bathymetry (also called coastal or shallow bathymetry) very important. Coastal areas are very dynamic and can change with erosion, flood etc. (Misra et al., 2018, Casal et al., 2020), creating a need for frequent bathymetry measurements of the same areas. The most commonly used methods for bathymetric mapping are carried out from boat or planes, making them time consuming and expensive. Especially boat based methods are limited, as they are not always able to reach the shallow water closest to the coast. Methods for deriving bathymetry from satellite data have also been developed, and with high resolution data freely available, the satellite based methods can provide cheap near-shore bathymetric maps, with a wide coverage (Geyman and Maloof, 2019).

1.2 Satellite based methods for bathymetric mapping

The Ice, Cloud, and Land Elevation Satellite-2, ICESat-2, is a satellite carrying a single instrument, ATLAS, with a photon-counting LIDAR. The satellite was launched in September 2018, and even though it was not part of the mission goal, studies have shown that the ICESat-2 LIDAR can be used for bathymetric mapping (Parrish et al., 2019, Ma et al., 2020). The study by (Parrish et al., 2019) presented the first early orbit validation of ICESat-2 bathymetry and they developed and tested a refraction correction in their work. They found ICESat-2 bathymetric mapping to be a promising new tool to assist in nearshore bathymetry. However, more knowledge of how well ICESat-2 is able to measure seafloor depths is still valuable. The drawback of ICESat-2 bathymetry, is that the data is collected along tracks, making it hard to get wide surface coverage for bathymetric maps.

In an effort to remedy this limitation, satellite bathymetry from optical imagery was considered and implemented in this project. With multi-spectral bathymetry the physical property that light attenuates in water is used to explain the relationship between reflectance and depth (Geyman and Maloof, 2019). Many multi-spectral bathymetry methods require prior knowledge of the depths in the area of interest. Therefore it can only be used in areas that have already been mapped to some extent, or it will require new measurements to be taken. With ICESat-2 bathymetry, it is possible to measure seafloor depths in the area of interest, and use them as the input in the multi-spectral bathymetry model, enabling a fully satellite derived bathymetry method. This has already been attempted using Sentinel-2 images and ICESat-2 by (Ma et al., 2020). In their study a point cloud processing algorithm was used to estimate bathymetry from ICESat-2, and they also implemented the refraction correction developed by (Parrish et al., 2019). They tested two multi-spectral methods for modelling bathymetry, the linear band model and the ratio band model. Both methods showed promising results. The linear band model and Sentinel-2 imagery will also be used in this project, as it provides high resolution images in the required bands.

1.3 Project goals

This project aims to test the capabilities of ICESat-2 for bathymetric mapping as well as the combination of ICESat-2 and Sentinel-2 for satellite derived bathymetry. The project was carried out in cooperation with the department Mapping & GIS at NIRAS, who provided single beam echo sounding data for islands in the Maldives. This ensured a perfect study area for the project, where we would be able to validate the results. The project will try to answer the questions:

- Is ICESat-2 LIDAR a good supplement for bathymetric mapping?
- How accurately can ICESat-2 determine the depth of the seafloor?
- How deep can ICESat-2 LIDAR penetrate?
- Can a combination of ICESat-2 and Sentinel-2 result in bathymetry with an accuracy comparable to current methods?
- How do the methods compare to non-satellite based methods?

The conventional bathymetric mapping methods will be reviewed shortly in chapter 2, as well as a more detailed description of the methods used in this project. The study area will be introduced in chapter 3. The satellites used will also be

presented, and the details of the data and data acquisition in the project will explained as well.

Then the pre-processing steps for both the ICESat-2 data and Sentinel-2 data will be presented in chapter 4.

The resulting bathymetry data will be validated using the single beam echo sounding data in chapter 5. Limitation of the validation and the maximum depth penetration will also be discussed. Additionally the ICESat-2 bathymetry will be used as input in a multi-spectral bathymetry model, together with optical image data from Sentinel-2. The satellite derived bathymetry will also be validated, and the advantages and disadvantages of combining ICESat-2 and Sentinel-2 for bathymetry will be discussed. Finally ideas for future work will be presented in chapter 7.

2 Bathymetric Mapping

Bathymetry is the study of underwater seafloor depths. The need for measuring bathymetry has been around for a long time. It is especially important for ship navigation, but also used for flood prevention, coastal monitoring, climate change protection amongst many other things.

Near-shore bathymetry is the focus of this project, as it is still considered difficult to map water depth in very shallow waters, and it is also time consuming and expensive to gain high accuracy maps (Parrish et al., 2019, U.S. Geological Survey, 2021).

There are many methods for measuring near-shore bathymetry. The oldest methods, going as far back as 3000 years, included standing with a pole in shallow waters or throwing weighted lines off boats. These methods are very limited and it would of course take a long time to get substantial coverage.(Wölfl et al., 2019)

Today another boat based methods is used. One of the most popular methods for bathymetric mapping is using an echo sounder on boats, which is able to cover a substantial area with high accuracy. There are two methods: single beam echo-sounders and multi beam echo-sounders (Wölfl et al., 2019). The general idea behind both methods is the same, a sound wave is emitted from an echo sounder (attached to the side of a boat) and the two-way travel time is used to determine the water depth. However, boat based methods are time consuming and expensive.

Airborne methods for bathymetric mapping have also been used, such as airborne LIDAR. This is also expensive, just like boat based methods, but it is possible to cover large areas and there are no limitations to how close to the coast it is possible to measure. This method is not able to measure as deep as SBES and MBES and is more dependent on clear waters, with an accuracy of up to 15 cm (Gao, 2009).

Then there are methods for mapping bathymetry using satellite data. Methods for using multi-spectral images have been developed and used since the 1970's, but LIDAR bathymetry from ICESat-2 is a new method that can also be used. The

advantage of using satellite data, is that there are many free data sources that can easily be accessed. This makes it possible to cover large areas without the need to travel to the area you want to map, making it much cheaper and less time consuming. It also makes it much easier to revisit the same area, as changes in bathymetry can occur, especially in areas with a soft bottom type, where erosion can change the seafloor drastically (U.S. Geological Survey, 2021, Wöfl et al., 2019, Lyzenga et al., 2006). Weather is a limitation, since these methods utilise optical light which is unable to penetrate clouds. Therefore the satellite has to cross the area of interest when the sky is clear of clouds.

This project is focused on the use of satellite data for bathymetric mapping. The use of LIDAR and multi-spectral images for bathymetry will be explained in greater detail in the following sections.

2.1 LIDAR Bathymetry

The general principles of LIDAR bathymetry are the same whether it is airborne or satellite based. Simply put, LIDAR measures the height of the seafloor by measuring the time it takes for a laser beam to return to the instrument. Bathymetric LIDAR is often a green laser (532 nm), and most airborne LIDAR missions also carry an infrared to measure the height of the water surface (Irish and White, 1998, Wozencraft, 2002). The maximum water penetration is found when using a laser with wavelength 532 nm. If the laser has a longer wavelength it is more prone to absorption by water. Shorter wavelength have another issue, since they will encounter stronger scattering and absorption by in-water constituents (such as dissolved gasses and minerals), resulting in shallower depth penetration. For those reasons, the green LIDAR is the most used (Gao, 2009). The infrared laser is not able to penetrate the water making it ideal for measuring the water surface height (Quadros et al., 2008). However it is also possible to determine the height of the water surface using the green laser (Parrish et al., 2019).

If an infrared laser is included, the depth is found as the difference between the return time of the signals, while if only a green laser is used, both the seafloor and water surface must be identified separately to estimate the depth. This requires more time when processing the data.

If ideal conditions are present, airborne LIDAR bathymetry can measure depths of up to 60 meters (Quadros et al., 2008), but in most cases it will be able to penetrate 25-40 meters. The LIDAR on the ICESat-2 satellite has been seen to

penetrate 0.96 Secchi depths (Secchi depth is the maximum depth that can be seen optically) by (Parrish et al., 2019), where the maximum observed depth was 38 meters. For comparison, some echo sounder systems can penetrate down to 3600 meters depth (KONGSBERG MARITIME, 2021). LIDAR is not able to replace echo sounder systems, however they offer a great addition, especially in the very shallow waters where echo sounders are not able to gain access.

2.1.1 Refraction

As LIDAR penetrates the water, it is also affected by refraction. Since the speed of light is different in air and water, the laser will refract when it hits the water. This results in both a vertical and horizontal displacement. A method to correct for this has been proposed by (Parrish et al., 2019) to be used on ICESat-2 LIDAR.

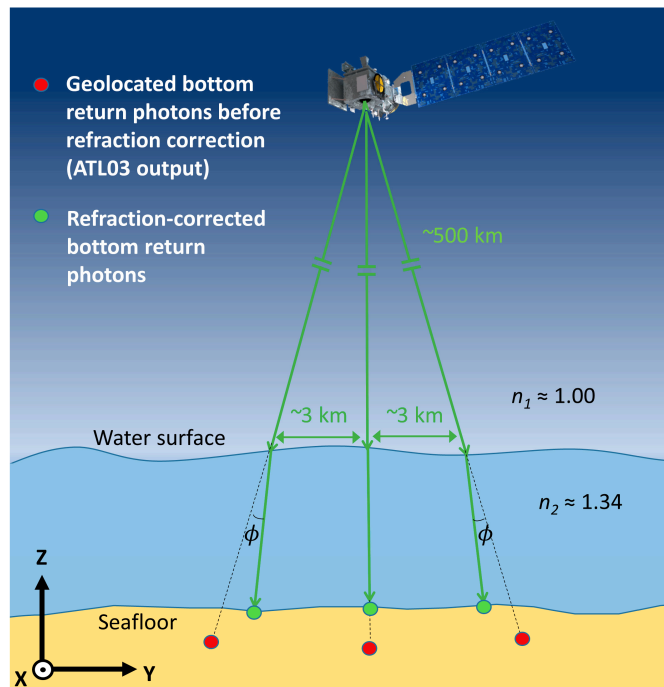


Figure 2.1: Visualisation of ICESat-2 photon refraction in water (Parrish et al., 2019)

In figure 2.1 the refraction of photons (that make up the laser beam) in water is visualised. Since the LIDAR instrument does not know whether the measured return photon has gone through water or not, an error is introduced. The photons are geolocated based on the return time and the assumption that they follow a straight line the entire way. However, when the laser beam penetrates the water, the beam is slowed down and the beam will also "bend" due to the reduced

speed. This is illustrated in figure 2.1 as the red and green dots. The red dots are the geolocation ICESat-2 assumes the seafloor has, while the green dots are where the photons actually hit the seafloor.

With the refraction correction which will be described below, it is possible to compute both vertical and horizontal corrections. The variables introduced in the equations are illustrated in figure 2.2.

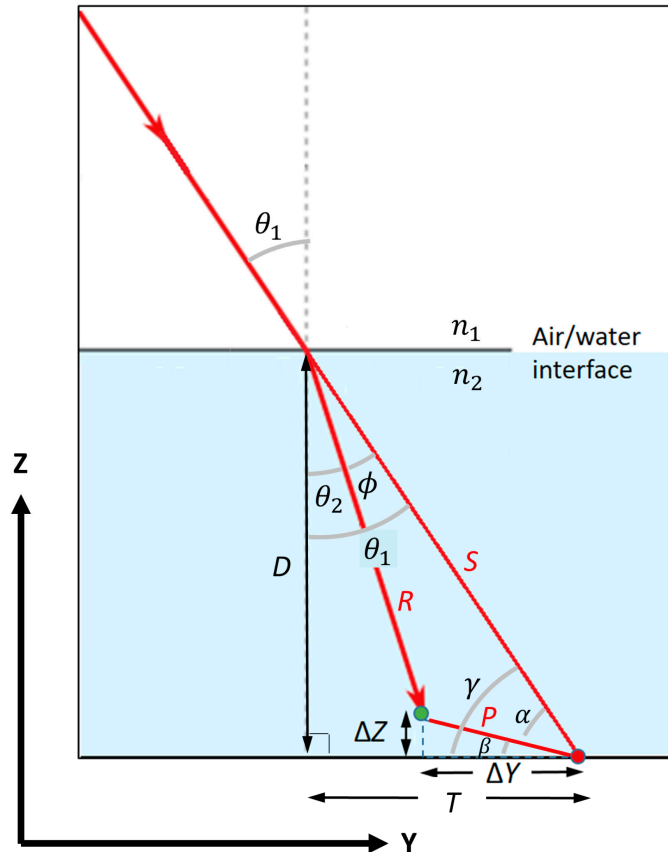


Figure 2.2: Visualisation of ICESat-2 photon refraction in water (Parrish et al., 2019)

The depth, D , is the distance between the water surface and uncorrected bottom return photons (how this is found is described in section 4.1). The angle of incidence, θ_1 , can be found as:

$$\theta_1 = \frac{\pi}{2} - \text{ref_elev} \quad (2.1)$$

where ref_elev is the elevation of the unit pointing vector for the reference photon. This value is included in the ICESat-2 data.

From the angle of incidence we can find the refraction angle, θ_2 . The refraction

angle is also dependent on the refractive index of air, n_1 , and water, n_2 . The refractive index of air is known to be 1.00029. The refractive index of water depends on salinity, temperature, pressure and wavelength of the laser. In (Parrish et al., 2019) they use a default value for salt water, with the assumption that the pressure is at 1 atmosphere, the water temperature is 20 °C, the salinity is 35‰ and the wavelength is 540 nm.

$$\theta_2 = \sin^{-1} \left(\frac{n_1 \sin \theta_1}{n_2} \right) \quad (2.2)$$

From the law of cosines we can find the slant range to the uncorrected bottom return photon, S , as a function of D and θ_1 .

$$S = \frac{D}{\cos \theta_1} \quad (2.3)$$

The corrected slant range, R , which is the actual distance the photon traveled through the water, can be found from the relationship between S , n_1 and n_2 . This is to account for the different speed of light in water.

$$R = \frac{Sn_1}{n_2} \quad (2.4)$$

Another variable that is needed for the correction is the angle β (see figure 2.2 for reference).

$$\beta = \gamma - \alpha \quad (2.5)$$

β is found as the difference between the two angles γ and α . Since the triangle where γ is one of the three angles, is a right-angled triangle, the angle can be found as

$$\gamma = \frac{\pi}{2} - \theta_1 \quad (2.6)$$

α is found in the triangle made up by the sides R , S and P , and from the law of sines it can be found as

$$\alpha = \sin^{-1} \left(\frac{R \sin \phi}{P} \right) \quad (2.7)$$

Finally the distance between the corrected and uncorrected photon return, P , is found by using the law of cosine

$$P = \sqrt{R^2 + S^2 - 2RS \cos(\theta_1 - \theta_2)} \quad (2.8)$$

The horizontal corrections can then be found as ΔY and the vertical offset as ΔZ .

These are the offsets that can be seen in figure 2.2. Y and Z are in a satellite centered coordinate system, and in order to add the correction to the coordinates of the bottom return photons, they must be projected onto a local (E,N) coordinate system. In order to do this, the azimuth of the unit pointing vector is needed. This is written as κ , and found as parameter *ref_azimuth* in the ICESat-2 data.

$$\Delta Y = P \cos \beta \quad (2.9)$$

$$\Delta Z = P \sin \beta \quad (2.10)$$

$$\Delta E = \Delta Y \sin \kappa \quad (2.11)$$

$$\Delta N = \Delta Y \cos \kappa \quad (2.12)$$

Once the horizontal correction has been projected onto the (E,N) coordinate system, we have a correction in the vertical direction (Z) and in the east (E) and north (N) direction. The corrected coordinates can be found as E' , N' and Z' .

$$E' = E + \Delta E \quad (2.13)$$

$$N' = N + \Delta N \quad (2.14)$$

$$Z' = Z + \Delta Z \quad (2.15)$$

Without this correction the photon returns could have up to 9 cm errors at 30 meters, and it is therefore an important thing to account for, if the aim is to have high accuracy. The refraction error will be larger at larger depths, so it is especially important when dealing with deeper waters.

2.2 Satellite Derived Bathymetry using multi-spectral images

Another satellite based method for bathymetric mapping is multi-spectral bathymetry, where optical imagery is used. This method utilises the relationship between bottom reflectance and depth in shallow water. It often utilises the blue and green spectral bands, since they have the best ability to penetrate through the water (Gao, 2009). It is often referred to as satellite derived bathymetry. This might be confusing, since ICESat-2 LIDAR is also used to derive bathymetry from a satellite based instrument. Satellite derived bathymetry will be used to refer to the combined bathymetry method using both multi-spectral imagery and satellite LIDAR. The general method of utilising optical imagery for bathymetry estimates will be

referred to as multi-spectral bathymetry.

Multi-spectral bathymetry can be split into two methodologies: empirical models and physics-based models. Both models rely on the physical knowledge of light through water. However, for empirical models, known bathymetry data points are needed. Physics-based approaches can be applied without knowing anything about the bathymetry, but they are more challenging to implement and require more computational power. Therefore empirical approaches are still commonly used for deriving bathymetry (Casal et al., 2020) and the method used in this project will also be empirical.

The most commonly used empirical methods are the linear band model (LBM) proposed by (Lyzenga et al., 2006) and the band ratio model (Stumpf et al., 2003). The LBM has been adapted and used by many for bathymetric mapping, because it is efficient and simple (Geyman and Maloof, 2019). However, both the LBM and the band ratio model are limited by the fact that they are unable to fully accommodate variable bottom types. Other methods for utilising the properties of optical imagery for bathymetry have also been proposed such as using a support vector machine method (Misra et al., 2018) or cluster-based regression (Geyman and Maloof, 2019). Even though these methods have shown promising results, the LBM still outperforms other methods in certain cases. Since the LBM is a well recognized model, that will also be simple to implement, it was chosen for this project.

2.2.1 Linear Band Model for estimating bathymetry

The linear band model proposed by (Lyzenga et al., 2006) assumes that a linear relationship between the water depth and log-transformed radiances exists. The model works best in clear water and with a homogeneous bottom type, as variability in the reflectances causes large errors. This is accounted for by including multiple bands in the model, making it less sensitive to variable bottom albedo. In theory, if more bands are used, a larger range of variations can be tolerated. The best results are achieved when using atmospherically corrected images (Vahtmäe and Kutser, 2016). The model uses satellite images at different optical bands. In situ measurements are also needed to estimate depth using the LBM.

The derivation behind the LBM can be found in (Lyzenga et al., 2006). The resulting model for estimating depths H can be described as

$$H = h_0 - \sum_{j=1}^N h_j X_j \quad (2.16)$$

for N optical bands. h_0 and h_j are variables defining a linear relationship between X_j and depth. They can be found via a regression analysis using in situ depths. The variable X_j is defined by (Lyzenga et al., 2006) as

$$X_j = \ln(R_j - R_{wj}) \quad (2.17)$$

where R_j is the above surface radiance in band j , and R_{wj} is the average deep water radiance. The radiances are log-transformed to create a linear relationship between input radiance and depth. The issue with this version of X_j , is that if some of the above surface radiance's have a lower intensity than the deep water radiance, the product $R_j - R_{wj}$ would be negative, resulting in imaginary X_j values. To account for this (Bramante et al., 2013) proposed a different X_j

$$X_j = \ln(nR_j) \quad (2.18)$$

where n is a fixed constant. For consistence with (Vahtmäe and Kutser, 2016 and Bramante et al., 2013) $n = 1000$ is used.

2.2.2 Implementation of Linear Band Model

In order to use the linear band model (LBM) for estimating depths, the parameters h_0 and h_j have to be found. The linear band model is set up as an inverse problem to find the model parameters, which can then be used in a forward problem to find the depths in the entire scene covered by multi-spectral satellite imagery. This project used Sentinel-2 imagery as the multi-spectral band data and ICESat-2 LIDAR estimated bathymetry will be used as the known depth (instead of in situ measurements). The pre-processing of these data is described in section 4.

The inverse problem can be solved in many ways, but in this project the problem was solved using both a least squares method and a damped least squares method. The two methods were tested in order to determine which was the best choice.

The LBM can be described as a forward problem, which can generally be written as

$$\mathbf{d} = \mathbf{Gm} \quad (2.19)$$

where \mathbf{m} is the model we want to find, \mathbf{d} is the data, in this case depths, and \mathbf{G} is a kernel matrix. In an inverse problem we first solve for \mathbf{m}

$$\mathbf{m} = \mathbf{Gd} \quad (2.20)$$

The LBM described in section 2.2.1 is defined by equation 2.16 and 2.18.

$$H = h_0 - \sum h_j X_j$$

$$X_j = \ln(nR_j)$$

h_0 and h_j are constants defining a linear relationship between X_j and depth H . The model parameters that we want to estimate are h_0 and h_j for each band that we use. If 3 bands are used, that results in 4 model parameters.

$$\mathbf{m} = \begin{bmatrix} h_0 \\ h_1 \\ h_2 \\ h_3 \end{bmatrix} \quad (2.21)$$

The \mathbf{d} in the forward model will be the estimated depth for each pixel in the multi-spectral image used, and the \mathbf{d} in the inverse problem is the in situ depth. \mathbf{d} can be defined as a collection of depths, either the known or estimated depth from pixel 1 to pixel p .

$$\mathbf{d} = \begin{bmatrix} H_1 \\ H_2 \\ \cdot \\ \cdot \\ H_p \end{bmatrix} \quad (2.22)$$

When training the model, each pixels with a corresponding in situ depth are extracted from each band. In the forward model all pixels are used to build the model. The kernel matrix \mathbf{G} can be written as

$$\mathbf{G} = \begin{bmatrix} -1 & X_1^1 & X_2^1 & X_3^1 \\ -1 & X_1^2 & X_2^2 & X_3^2 \\ \cdot & \cdot & \cdot & \cdot \\ \cdot & \cdot & \cdot & \cdot \\ \cdot & \cdot & \cdot & \cdot \\ -1 & X_1^p & X_2^p & X_3^p \end{bmatrix} \quad (2.23)$$

Where p is the number of pixels used (this will be smaller when training the model, and will be the total amount of pixels in the image when building the full model). X_1^2 is $\ln(nR_1^2)$, where R_1^2 is the reflectance in the second pixel of the first band. The model is set up, such that each row in \mathbf{m} , \mathbf{d} and \mathbf{G} correspond to the linear band model in equation 2.16. When solving this as a system of many equations with many H values, the least squares method or damped least squares method will estimate the model parameters in \mathbf{m} , so they best describe the linear relationship between all the known depths and pixel reflectances in the multi-spectral image. The least squares solution for finding \mathbf{m} is defined as

$$\mathbf{m}_{LS} = (\mathbf{G}^T \mathbf{G})^{-1} \mathbf{G}^T \mathbf{d} \quad (2.24)$$

and the damped least squares can be written as

$$\mathbf{m}_{DLS} = (\mathbf{G}^T \mathbf{G} + \alpha^2 \mathbf{I})^{-1} \mathbf{G}^T \mathbf{d} \quad (2.25)$$

\mathbf{I} is an identity matrix and α is the dampening parameter. It can be estimated in many ways. In this project, α was estimated using an L-curve. The aim of the L-curve is to find the model with the smallest model norm and model misfit (residuals). You can have a smaller model norm with a larger model misfit and vice versa, however the damped least squares method tries to find the best trade-off between the two. The normal least squares only tries to minimize the model misfit.

Summarizing, we have known depths that correspond to some of the pixels in the multi-spectral image. This is used to train the model, in order to find the model parameters in \mathbf{m} . This is set up as a system of equations and solved as an inverse problem, using either the least squares method or the damped least squares method. The resulting model parameters can then be used, together with the pixel values in each of the multi-spectral bands, to estimate a depth in each image pixel.

2.3 Echo Sounders

Single Beam Echo-Sounders (SBES) and Multi Beam Echo-Sounders (MBES) are popular methods for mapping bathymetry, as they have high accuracy and can

penetrate down to 3600 meters depth (KONGSBERG MARITIME, 2021, Wöfl et al., 2019). The accuracy has been found to be between 3-30 cm (Ernstsen et al., 2006).

Echo sounders work by emitting a sound wave and measuring the two-way travel time, in order to determine the water depth. The echo sounder is usually operated from a boat, with a GNSS receiver on board measuring the exact location of each sounding. With MBES a fan (or multiple beams) of sound is emitted, allowing for mapping of a larger area at the time. SBES is often used for smaller water bodies, where MBES is used for larger areas. The challenge with boat based echo sounding methods, is the danger involved with operating the boat in shallow waters. This has prompted the National Oceanic and Atmospheric Administration to implement a policy of not surveying too close to the shore (NOAA, 2014). Another issue with echo sounding methods, is that it is time consuming since it requires sending a boat out to the area that needs mapping. This also makes the method expensive.

3 Study Area and Data

3.1 Study Area

The Maldives is an island country in South Asia, made up of 26 atolls. The chain of atolls stretches out over 871 km, crossing the equator. There are 1190 islands, most of them very small and no more than 2 meters above sea level (FAO, 2011). The Maldives was chosen based on the availability of high accuracy validation data around five islands, which was made available through collaboration with NI-RAS.

The bathymetry of the five islands has been mapped using single beam echo soundings, however only three of these islands are used in this project, since ICESat-2 data was only available for those islands.

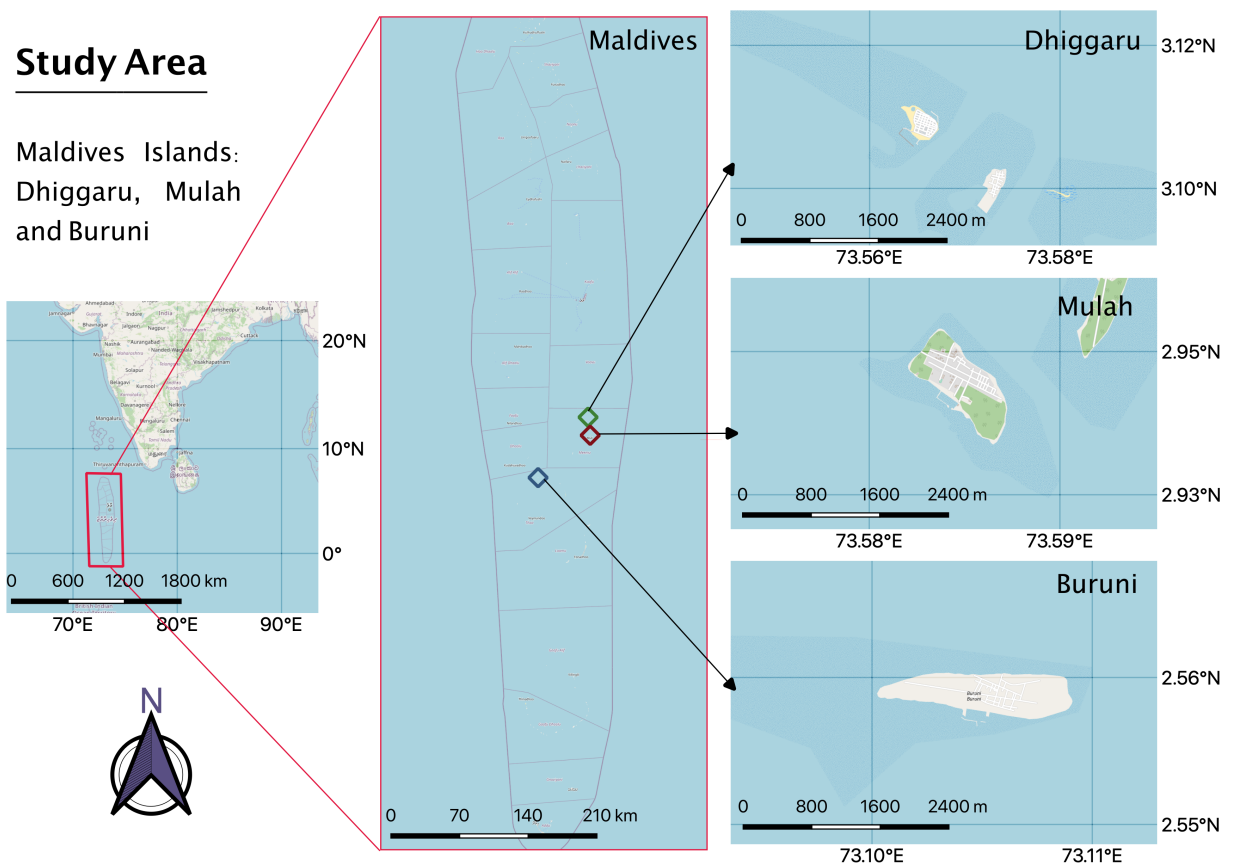


Figure 3.1: Map showing the location of three islands, in the Maldives, used as the study area

The Maldives is an ideal place to study bathymetry, as it has clear waters with Secchi depths measured to be between 15-34 meters near the capital Malé in the Kaafu Atoll (Knaap et al., 1991). This is not near any of the islands used in this project, however it is the only available measurements. It is assumed that the Secchi depth would be at least 20-30 meters around the selected islands (Bundgaard, 2020, personal communication).

In figure 3.1 the study area is presented. The Maldives is shown to be located south-west of India, close to the equator. The three islands: Dhiggaru, Mulah and Buruni are located fairly close to each other, and a closer look at the islands is also shown in the figure.

Dhiggaru and Mulah are both located in the Mulaku atoll. The atoll, like all other atolls, is made up of a ring-shaped coral reef. Both islands are located on the barrier reef (the outer ring reef), Dhiggaru is on the northern side of the atoll, while Mulah is on the east side of the atoll. The coral reef making up the atoll has several openings, with the only opening or channel on the eastern side being right next to Mulah. This channel is called Mullah Kanduu. There is another channel east of Dhiggaru called the Dhiggaru Kanduu. The channels are openings in the ring reef, making them much deeper than the reefs and creating a passage into the atoll for boats (themaldivesexpert.com, 2018).

It was not possible to find information on the specific corals and other bottom types that surround the three islands. From other atolls in the Maldives, it is known that inside the atoll there are many reef systems. Between the reef systems inside the atoll, it is assumed that the bottom is sand. Therefore it is possible that there is some sandy bottom around Dhiggaru, Mulah and Buruni as well. However it is mostly coral reefs, which we can assume are fairly hard and unchanging (Knaap et al., 1991, Bundgaard, 2020).

Buruni is located on the northern side of the Kolhumadulu Atoll, with an opening in the reef east of the island. Dhiggaru is ~500 m across, Mulah is ~1.35 km long and Buruni is ~1.45 km long (measurements based on satellite images). Satellite images of each island reveal the coral reefs and the openings in the coral reefs near each island in figure 3.2.

The Maldives has a tropical monsoon climate, with mean annual temperatures of 28 °C. The country is affected by monsoons, however rainfall is uniformly distributed throughout the year (FAO, 2011). The Maldives is a very sunny country, and it has 40 % more sunshine hours (or 1000 sunshine hours more) than Den-

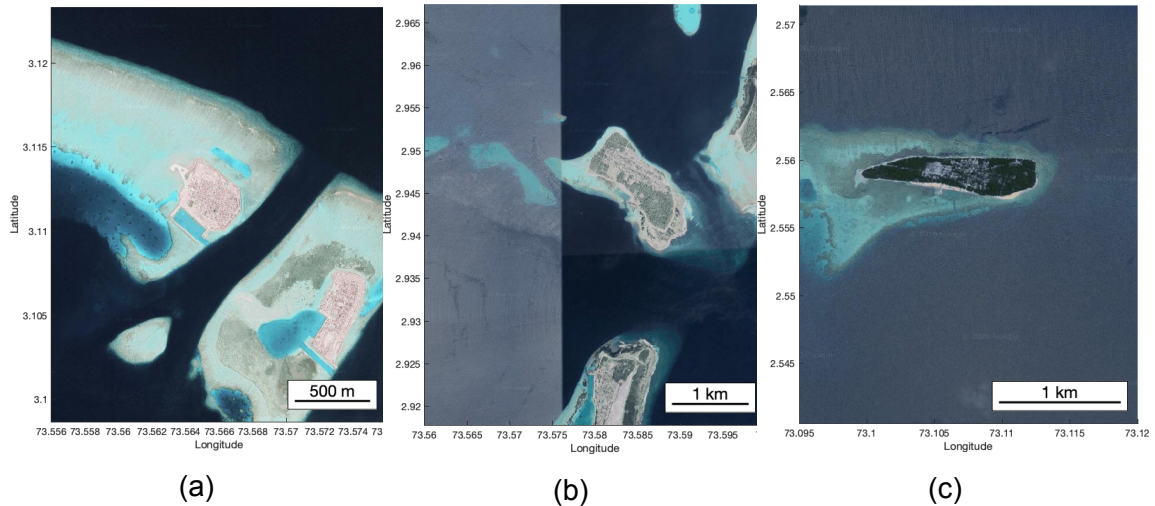


Figure 3.2: Satellite images showing a) Dhiggaru b) Mulah c) Buruni

mark (DMI, 2021, weatherandclimate.com, 2021). This increases the chance of imaging the study area from satellites.

3.2 Data

For this project data from both the satellite ICESat-2 and the satellite Sentinel-2 have been utilised. A short description of both satellites will be presented in this section, as well as the description of the data sets used from the two platforms. Finally, additional data sources used in the processing and validation will be introduced.

3.2.1 ICESat-2

Satellite

The Ice, Cloud, and land Elevation Satellite 2, ICESat-2, was launched September 15, 2018. On board, ICESat-2 carries a photon-counting laser altimeter, and it measures the elevation of ice sheets, glaciers, sea ice and more by sending out 10,000 laser pulses a second, resulting in a high resolution along the satellite track (Neumann et al., 2020). While the name and mission statement do not mention water or bathymetry, the photon counting laser is able to measure water surface heights and penetrate the water in order to see the underlying bathymetry in coastal areas (Parrish et al., 2019).

ICESat-2 carries a single instrument, the Advanced Topographic Laser Altimeter System (ATLAS). ATLAS measures the travel times of the laser pulses in order to calculate the distance between the spacecraft and Earth's surface. The laser light on ATLAS has a wavelength of 532 nm, green on the visible spectrum.

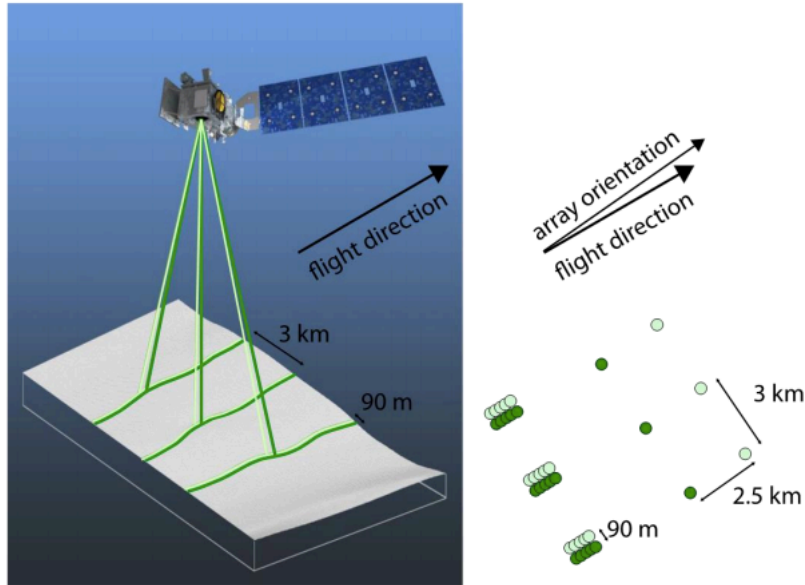


Figure 3.3: ATLAS idealized beam and footprint pattern (Neumann et al., 2020)

Each transmitted laser pulse from ATLAS is split by a diffractive optical element to generate six individual beams. The beams are arranged in three pairs, with each pair having a weak and a strong beam. The beam pairs have an energy ratio of approximately 1:4. In figure 3.3 the beam and footprint pattern is visualised. The three beam pairs are approximately 3 km apart in the across track direction, while the distance between the weak and strong beam in each pair is 90 m in the across-track direction, and 2.5 km in the along-track direction. As the satellite moves in the along-track direction, the collection of overlapping footprints create 6 ground beam tracks. Each ground beam track is numbered according to its position, with ground track 1L (GT1L) on the far left and ground track 3R (GT3R) on the far right. The first beam pair is GT1L & GT1R, the second GT2L & GT2R ect. As the satellite moves it traces out an imaginary Reference Ground Track (RGT), which is were ATLAS is pointing too. It gives an indication of the area the three beam pair will cover. The ICESat-2 mission acquires data along 1,387 different RGTs and each RGT has a 91-day repeat cycle (meaning it will revisit the same place every 91 days). Each beam footprint is approximately 17 meter in diameter. (Neumann et al., 2020)

Data

The level 2 product ATL03 will be used in this project. ATL03 contains time, latitude, longitude, and ellipsoidal height (WGS84) for each photon event. For each beam the data file contains information on height and geolocation, but also geophysical corrections. The heights are already corrected for several geophysical phenomena, such as effects of the atmosphere and solid earth deformation. All

corrections can easily be removed, and some effects, such as ocean tides can easily be added if needed. Each photon is also classified, based on surface type and signal photon confidence (either low, medium, or high confidence) (Luthcke et al., 2019). There was no need for removing photons based on surface type, and the signal photon confidence was not used to ensure that possible bathymetry was not accidentally classified as noise.

ATLAS splits the laser into six beams, which means that each time the ICESat-2 satellite passes over the study area, there are six beams that could potentially cover the specific area in question. The beams are in three pairs of two, with the three pairs being 3 km apart. So for the small islands that we are looking at in the Maldives, it is likely only one beam pair that is useful, for each data acquisition. There was validation data available for five islands, however for two of these islands there were no beam tracks close enough to the islands.

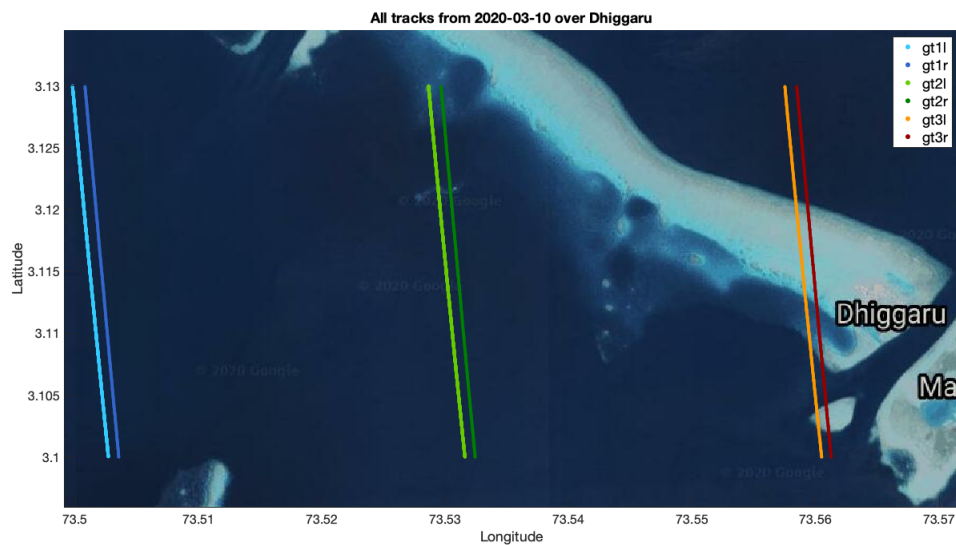


Figure 3.4: All tracks from 2020-03-10 in the area close to Dhiggaru

In figure 3.4 the six beams are shown from 2020-03-10. In this case, only the GT3L and GT3R beam tracks (red tracks) cross Dhiggaru. All data files (from October 2018 - November 2020) that had tracks in proximity of on of the islands were visually inspected to select the beam tracks that intersected with the islands. The data acquisition goes back to October 2018, and ~85 files were inspected for the project. The data was acquired from the The National Snow and Ice Data Center (NSIDC) website (NSIDC, n.d., Neumann et al., 2020). From all the potential dates, five beam pairs came close to Dhiggaru, eleven were close to Buruni and

six were close to Mulah.

Once all the beam tracks that cross each island have been identified, it is possible to see the extent of the coverage. In figure 3.5, all the tracks that came close to Dhiggaru are shown. Each of these tracks follow the same RGT, however off-pointings have resulted in the beam tracks being separated slightly. This allows for greater coverage.

The tracks only cover a small part of the coral reef around the island, however the tracks are close together in the covered area. The tracks with the same color are the weak and strong beam from the same date. The weak and strong beam pairs are 90 meters apart.

Some of the beam tracks in figure 3.5 are not continuous, such as the orange tracks. Data gaps can occur for many reasons, and some tracks that should have covered the area are completely absent, possibly due to cloud coverage.

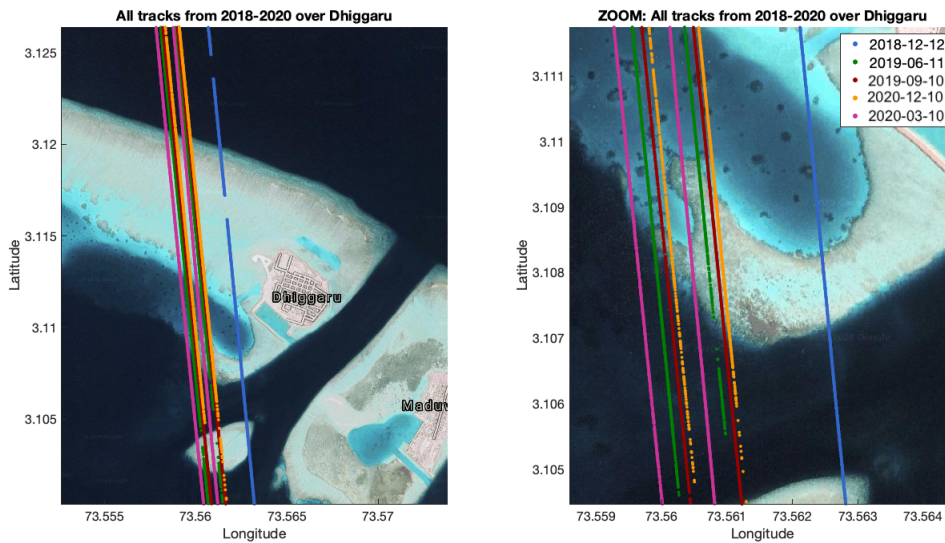


Figure 3.5: All tracks from ICESat-2 that come close to Dhiggaru

From the remaining nine tracks (from five dates) that cover Dhiggaru, they were each visually inspected to see if they contained possible bathymetry. The track from December 12th 2018 (blue) turned out to have no discernible bathymetry, leaving eight tracks with visible bathymetry, which have to be processed to get the seafloor depths. Buruni had 14 beam tracks from eight dates and Mulah had eight beam tracks from four dates, with discernible bathymetry. The tracks used for Dhiggaru and Mulah have Reference Ground Track 1141, and the tracks covering Buruni are from RGT 0257 and 0066.

The beam tracks used to estimate the bathymetry around Mulah and Buruni are shown in figure 3.6.

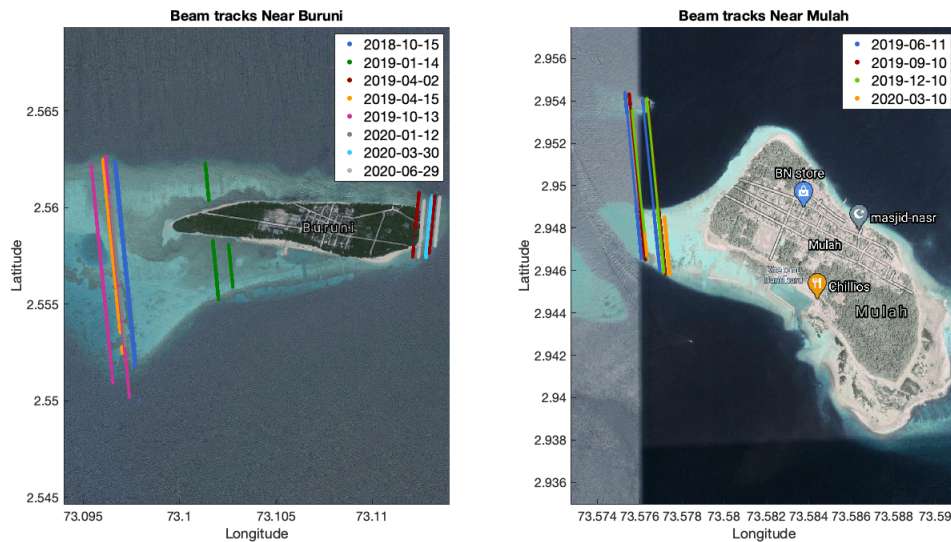


Figure 3.6: Beam tracks from ICESat-2 that come close to Buruni and Mulah with usable bathymetry data

3.2.2 Sentinel-2

Satellite

The Sentinel-2 mission is comprised of two polar-orbiting satellites, phased at 180° to each other. It has a wide swath of 290 km and a high temporal resolution. With one satellite there is a revisit time of 10 days at the equator, and when using both satellites the same area will be imaged every 5 days. The main instrument on-board the Sentinel-2 satellites is the MultiSpectral Instrument (MSI). The MSI works passively, by collecting sunlight reflected from the Earth. A push-broom sensor works by collecting rows of image data across the orbital swath, making use of the forward motion of the satellite. MSI measures the Earth's reflected radiance in 13 spectral bands from visible to short wave infrared (SWIR). Four bands have a spatial resolution of 10 m, six bands have a spatial resolution of 20 m, and the remaining three have a spatial resolution of 60 m. (ESA, 2015)

Data

Sentinel-2 data was taken from Copernicus Open Access Hub (ESA, 2020). The level-2A product was chosen, since an atmospheric correction has already been carried out, resulting in bottom of atmosphere (BOA) reflectance, instead of the

top of atmosphere (TOA) reflectance of the level-1C product. The level-2A product is not available for older data, however the atmospheric correction can be carried out in the Sentinel Application Platform (SNAP). The best result for the linear band model (LBM) is found when using atmospherically corrected images (Vahtmäe and Kutser, 2016). The data is downloaded in tiles of size 100 x 100 km. A single tile (T43NCD) covers both Dhiggaru and Mulah. While a second tile was necessary to also cover Buruni (T43NBC). Two identical Sentinel-2 satellites (2A and 2B) operate simultaneously, phased at 180° to each other. They have a slightly different spectral resolution. Only Sentinel-2A was used in this project.

For the LBM, if a larger number of bands is used, theoretically a larger range of variations in bottom type can be tolerated (Vahtmäe and Kutser, 2016). However, MSI only measures three visible bands a 10 m resolution. If more bands were to be included, it would be at the expense of the high spatial resolution. Many other studies have also successfully estimated bathymetry using the LBM with bands in blue, green and red (Ma et al., 2020, Casal et al., 2020, Misra et al., 2018). Therefore these are the three bands that will also be used in this project.

Band number	Spectral resolution	Spatial resolution
2	Blue (492.4 nm)	10 m
3	Green (559.8 nm)	10 m
4	Red (664.6 nm)	10 m
8	NIR (832.8 nm)	10 m
12	SWIR (2202.4 nm)	20 m

Table 3.1: Sentinel-2 bands B02, B03, B04 and B12. Spectral resolution is the central wavelength.

The spectral bands utilised for the project are described in table 3.1. Where B02, B03 and B04 are the blue, green and red bands respectively, B08 is near infrared (NIR) and B12 a slightly coarser SWIR band. The SWIR band B12 will be used for a land and cloud mask, while NIR will be used for sun-glint removal.

In figure 3.7 a subset of a Sentinel-2 image is shown, in four of the spectral bands (B02, B03, B04 and B12). It is easy to see that land and clouds have a significantly different pixel value than water in the SWIR band. Several images from different

dates were inspected to find one with the smallest amount of cloud coverage. Ultimately two image tiles from 2020-06-30 were chosen to cover the three islands.

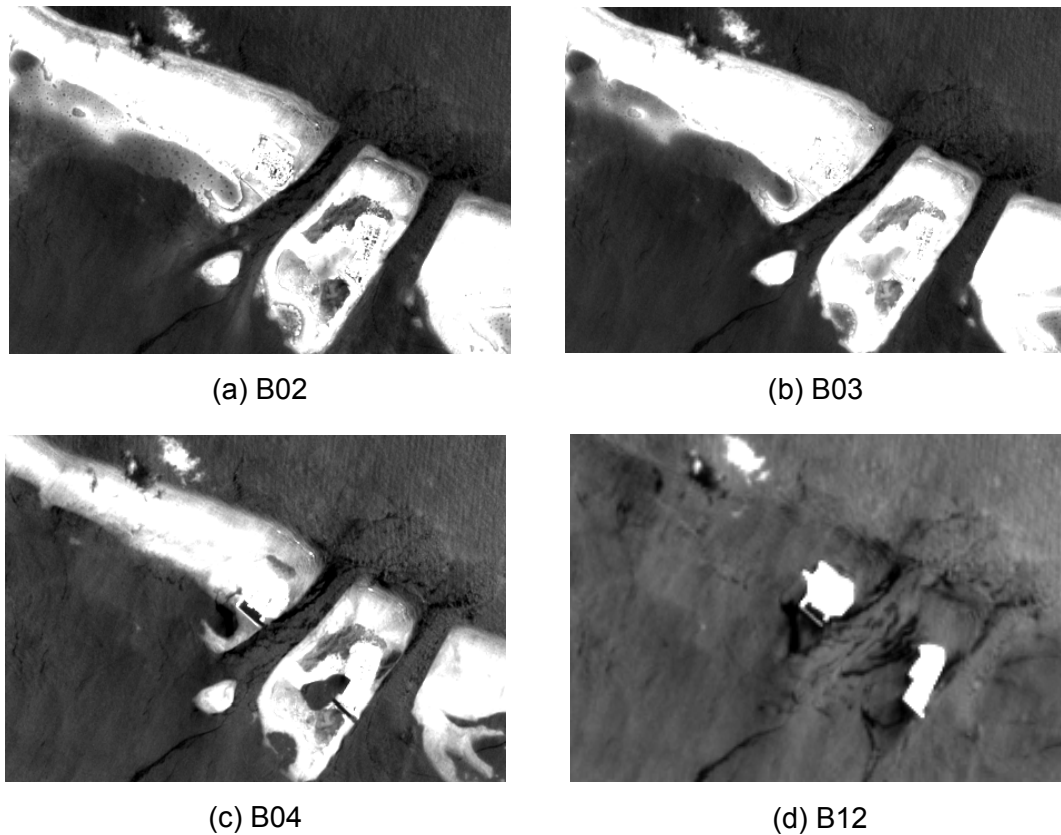


Figure 3.7: Subset of Sentinel-2 image from 2020-08-19 (Showing the island Dhiggaru)

3.2.3 Single Beam Echo Sounding

Single beam echo sounding data was collected around Dhiggaru, Mulah, Buruni and two other islands in the Maldives, and made available for this project by the consultancy firm Riyan Private Limited (Abid, 2020), through collaboration with NIRAS. The single beam data is the best measurements of depths around these islands, and therefore the ideal data to use for validation. The accuracy is assumed to be 5-10 cm for the measured depths, with the accuracy decreasing with depth (Bundgaard, 2020, personal communication).

In figure 3.8 satellite images of the 3 islands are shown. For each island we see a satellite image with the single beam data shown on top. The data is collected by boat, and the images clearly show the track the boat followed. The colourbar illustrates the depths in the areas.

Dhiggaru is shown in figure 3.8a, where the depths are measured down to 75 meters. The majority of the covered area however, is 0-10 meters deep, with the water outside the atoll (north of the island) being the deepest. In figure 3.8b we see Mulah. The depths around the island are between 0-75 meters, and not surprisingly, the water is more shallow close to the coast and deep further away from the island. The shallow area appears to be smaller than for Dhiggaru. Buruni also has a large area with depths ~5-10 meters, and a drop to much deeper waters outside the coral reefs north of the island.

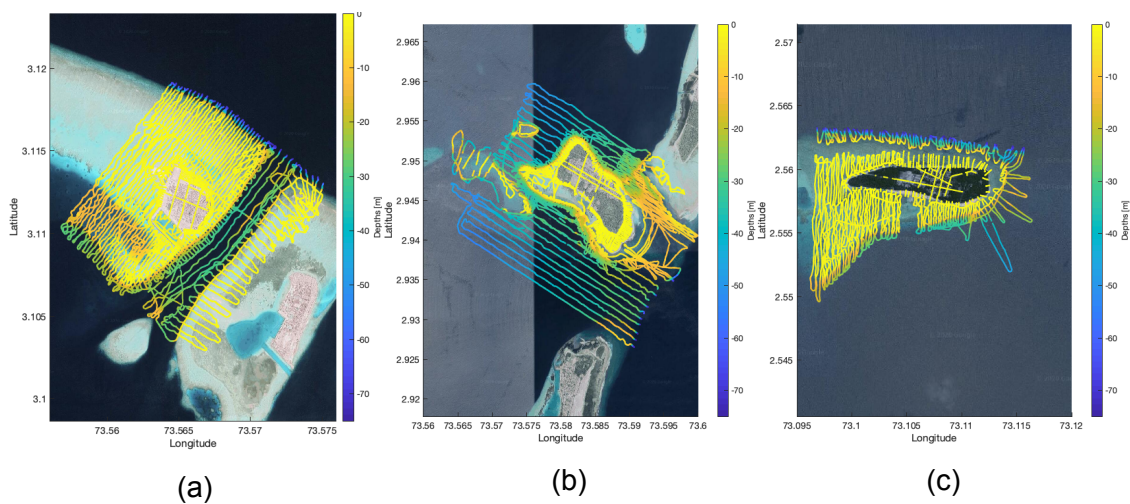


Figure 3.8: Satellite image of with single beam data tracks and depth values a) Dhiggaru b) Mulah c) Buruni

3.2.4 Mean Sea Level data

The mean sea level (MSL) is used as reference height for all measured depths. Since the single beam depths are given in reference to the local MSL for each island, the same will be done for the depths estimated in this project for easy comparison. The photon height data in the ICESat-2 ATL03 data set is given in reference to the WGS84 ellipsoid, so it was decided to find the MSL around each island in WGS84. The MSL information comes from the DTU15MSS (Mean Sea Surface) model (Andersen, 2015), and the MSL for each island is shown in table 3.2.

Island	Dhiggaru	Mulah	Buruni
MSL (WGS-84)	-96.037 m	-96.184 m	-94.771 m

Table 3.2: MSL in WGS84 in reference to the DTU15MSS model

4 Methods and Data processing

The pre-processing steps for both the ICESat-2 and Sentinel-2 data is presented in this chapter. The method for combining the data from the two satellites for a satellite derived bathymetry model is shortly described as well.

4.1 ICESat-2 LIDAR

The data set used for the ICESat-2 bathymetry estimates, is the ATL03 data set. ATL03 contains heights above the WGS84 ellipsoid, latitude, longitude, and time for all photons. Tracks that overlap with the area of interest are identified, and the ones that appear to have bathymetric information go through the processing steps described below. The tracks chosen for each island are described previously in section 3.2.1.

Drawing inspiration from (Parrish et al., 2019), the processing of the photon data from ATL03 is split into several steps:

1. Separate seafloor and water surface
2. Define water surface
3. Correct for refraction
4. Tide correction
5. Remove outliers and define smooth bathymetry profile

Most of the processing steps require manual decisions. Since the goal of the project is to test how well the ICESat-2 LIDAR is able to measure depths, and to use the ICESat-2 bathymetry as input in a LBM for satellite derived bathymetry, it was not prioritised to create a fully working automated process.

4.1.1 Separate seafloor and water surface

To illustrate the data processing steps, the GT3R beam track crossing Dhiggaru on 2020-03-10, will be used.

To separate the seafloor photons and the water surface, a manual inspection was used. Photon height and coordinates from an ATL03 data file were extracted in a small area around the islands of interest. The photon height is plotted as a function of latitude in figure 4.1. The water surface and seafloor can be spotted already in this unprocessed profile. The water surface will always have a strong return and is assumed to be straight, so the straight line defined by a high density of photon returns, must be the water surface. Despite the noisy data, the

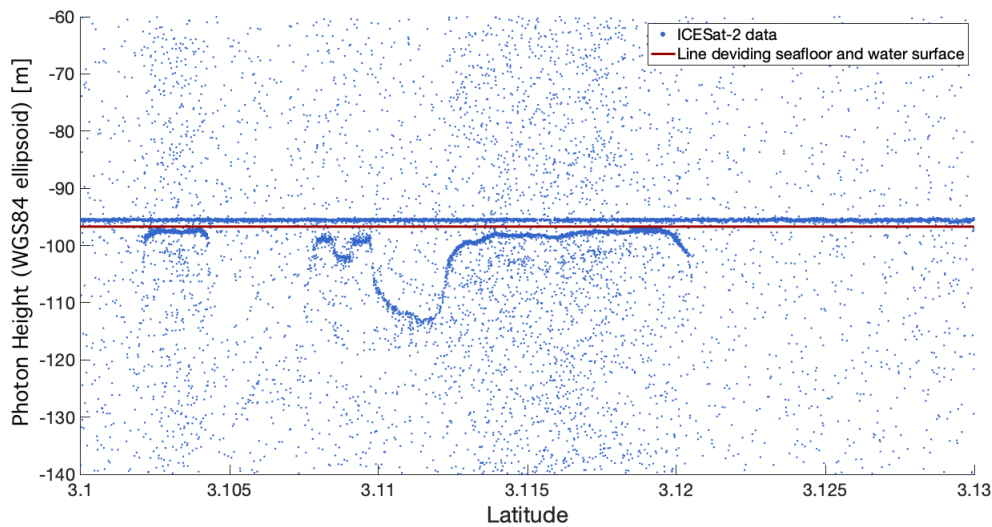


Figure 4.1: Bathymetry profile of beam GT3R across Dhiggaru from 2020-03-10.

bathymetry is fairly easy to see as well. Since the Maldives has very clear waters, the bathymetry is much easier to detect than it might be in murkier waters (where the Secchi depths are more shallow). The red line in figure 4.1 indicates the separation of the seafloor and water surface. In this project the separation was done manually, by defining the height in WGS84 that separates the water surface and seafloor.

4.1.2 Define water surface

The data above the red line in figure 4.1 is used to define the water surface height. We want to define the water surface height as the mean of the straight dense collection of points that clearly make up the water surface. In the profile shown in figure 4.1 there is a lot of noise, making it harder to automatically determine the water surface height. In the cases where there was a significant amount of noise in the data above the water surface, the water surface height was manually defined by drawing a straight line through the data points that make up the water surface and manually reading the WGS84 height of the line. In the case where the noise was less prominent, an outlier removal removed the small amount of noise around the water surface. This was done in a moving window, where outliers were defined as elements more than three local scaled MAD (median absolute deviation) from the local median. The water surface was then found as the average height of the remaining data points. This was possible to do for most of the data tracks, and was faster than having to define a line through the water surface points. The water surface height is found, because the depth from water surface to seafloor is needed in the refraction correction.

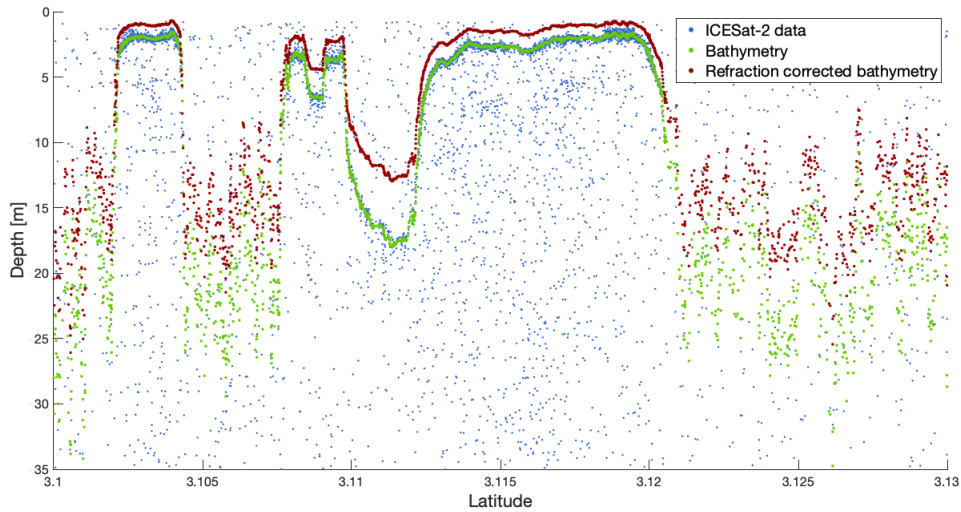


Figure 4.2: Illustration of effect of refraction correction (beam GT3R from 2020-03-10)

4.1.3 Tidal and Refraction correction

All data points below the red line in figure 4.1 are corrected for refraction and tides. Since the beam tracks used to estimate the bathymetry around all three islands are acquired on different days at different times, the tides will vary. For some tracks the water surface is above the MSL, and for others the water surface is below the MSL. In order to compare the measured water depths, they all need to refer to the same reference frame.

In figure 4.2 the data is corrected for tides. This is done by defining all depths in reference to the local MSL instead of the water surface. The MSL for the water around each island was found in WGS84, to easily implement it in this project, since the photon data is in WGS84. As an example, the MSL around Dhiggaru is -96.037 m in WGS84, so this MSL value is subtracted from all photon depths, resulting in the MSL=0 m in the new reference system. All depths were then defined as positive, since this was easier to work with going forward. The local MSL was found for each island, since this was the same reference point used in the single beam data that will be used for validation, making it easier to compare the two data sets.

The refraction correction described in section 2.1.1 is used, and the result can be seen as the red points in figure 4.2. Without refraction correction, the bathymetry would be found as the green points (both the red and green points have also been through outlier removal and have been smoothed out to make it easier to see them

in the figure). It is clear that the refraction correction has a significant influence on the seafloor depths, and that the effect is larger for deeper waters. To carry out the refraction correction, several variables are needed. The elevation and azimuth parameters are included in the ATL03 data file, and are easily implemented. A refractive index of water is also needed, and was chosen to be 1.34116, the same as used in (Parrish et al., 2019).

The refractive index of water in Maldives is affected by the warmer waters, since it is near the equator, and high salinity due to more evaporation in the warm climate. An increase in salinity will increase the refractive index, while warmer waters have the opposite effect. For this project the refractive index was first estimated using tables in (Leyendekkers, 1977). Later, the refractive index was found using the method described in (Quan and Fry, 1995), where the refractive index is found as a function of wavelength, temperature and salinity. The mean water temperature in Malé (the capital of the Maldives) is 29.1 °C (seatemperature.org, 2021) and the salinity is between 33.8-34.7‰ (University of Salento, 2011), and since we are looking at shallow water where there is more evaporation, the salinity is chosen to be 34.7‰ for the calculation. The wavelength of the laser is also needed, and that is 532 nm for ICESat-2. This resulted in a refractive index of 1.3402, which is slightly smaller than the one used in (Parrish et al., 2019). However, the difference in the refractive index found by either of the two methods compared to the refractive index used in (Parrish et al., 2019) would only result in depth errors as small as a few millimeters. This would not have a significant influence on the final result, so the refraction correction is carried out with the refractive index of 1.34116 in this project.

4.1.4 Outlier removal and smoothing

The blue data points in figure 4.2 represent the ICESat-2 data before any corrections are carried out. In order to extract only the bathymetry estimates, outliers are found and removed and the data is smoothed. Since there have been few attempts at using ICESat-2 for bathymetry, there is no standard way of determining which photons should be kept as bathymetry. A few studies have looked at ICESat-2 bathymetry, (Parrish et al., 2019) does not explain their method and (Ma et al., 2020) uses a point cloud processing algorithm for estimating seafloor photons. The latter method could have been used, however it would be slightly more complicated to implement. Therefore trial and error was used, to find the best procedure for the ICESat-2 tracks used in this project. For removing outliers, a moving window method was implemented. First a moving window with a size of 100 data points is used. This is equivalent to ~20 meters in a strong beam track and ~80 meters in a weak. This removes a good amount of the outliers, but especially in the areas of the bathymetry with rapid changes in depth, a smaller

window is needed. The smaller window of 30 data points (~5-10 meters for strong beam and ~25 meters for weak beam) will be able to find outliers within a smaller area, such that only the data points in areas with a high concentration is remaining. Outliers in this process are defined as elements more than three local scaled MAD (median absolute deviation) from the local median over a window. This was more robust than using three standard deviations from the mean, which was also tested. The process of removing outliers in a moving window with a size of 30 data points is done with 10 iterations. Only doing it once did not remove all outliers, however, 10 iterations appeared to remove a substantial amount of outliers without requiring a lot of computational time. A more refined method could possibly be implemented, but for this study area the method worked well enough.

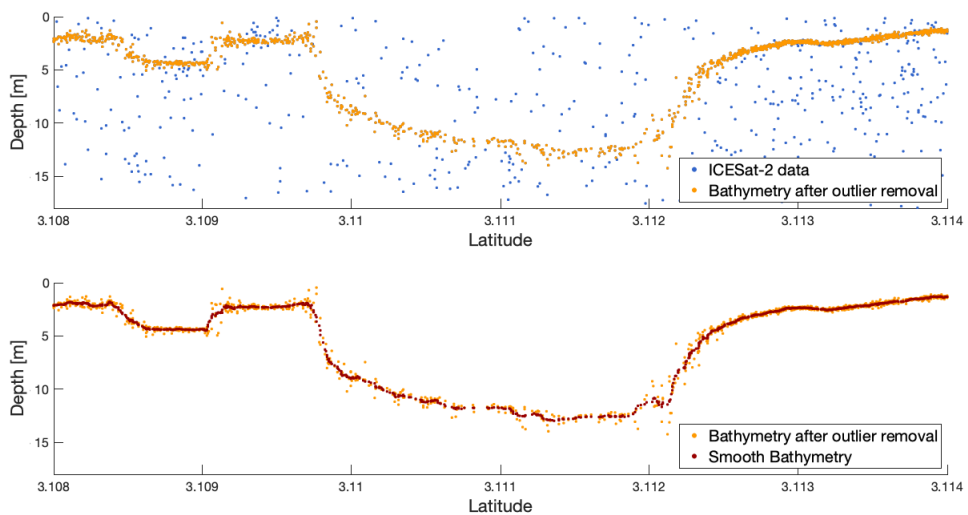


Figure 4.3: Outlier removal and smoothing of data in bathymetry profile (beam GT3R from 2020-03-10)

After removing outliers the data is smoothed using a moving average with 10 data points at the time. This is to find the mean depth at a certain point, instead of the small dense "cloud" of data points we are left with after outlier removal. The moving average is done in a small window, such that the areas where there is a rapid change of depth does not affect the result. In a large window the average might be effected by depths that are several meters away, while the small window ensures that only the surrounding data points effect the final depth estimate.

The outlier removal and smoothing of the data is visualised in figure 4.3. The top image shows the data before and after outlier removal (in a small subset of the

data also used in figure 4.1 and 4.2). At this point in the data processing the data points that appear to be bathymetry are easily discernible. After smoothing, the bathymetry estimates are less scattered, and the final bathymetry profile (the red line in the bottom image) is more clear than before the processing steps.

Another example of the data processing of a bathymetry profile is shown in figure 4.4 and 4.5 for beam GT3R from 2019-09-10. The data in this ICESat-2 track is less affected by noise, but the processing steps are still the same. The resulting bathymetry after processing is the red line in figure 4.5. In the left side of the bathymetry profile we see that the outlier removal and smoothing has only revealed noise, however in the raw data in figure 4.4, we see that there is an indication of bathymetry in the same area. This illustrates that the outlier removal used is not perfect, since it has removed data points that appear to be bathymetry. This can be handled by either manually extracting the data points or by improving the outlier removal process. During this project a few different things were tested, however no method was successful in removing the noise close to the water surface while also extracting the bathymetry that appears to be present in the very left side of figure 4.4.

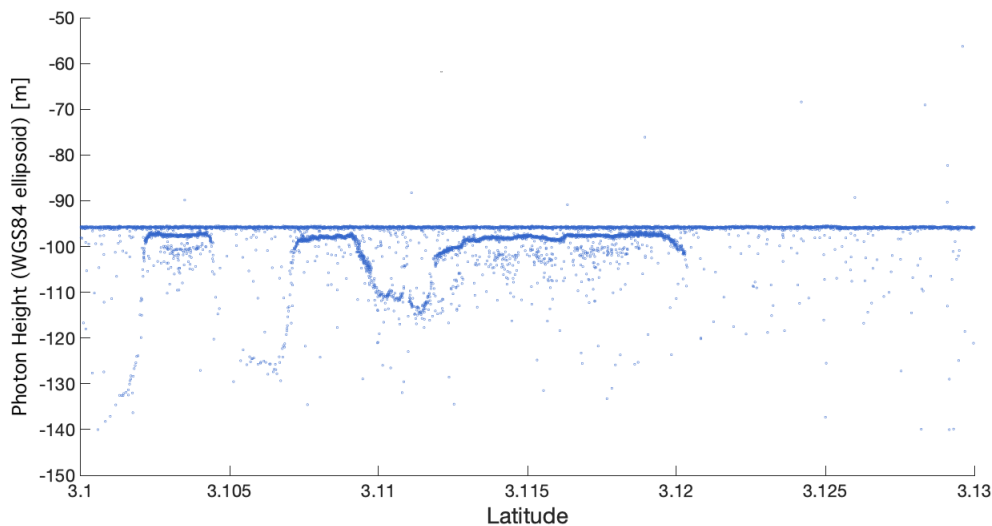


Figure 4.4: photon height data from ATL03 data file before data processing (beam GT3R from 2019-09-10)

After all the data processing steps, it is clear that there are areas in the profile that are not bathymetry. These are the areas with no clear bathymetry (or not clear enough for it to not be mistaken for noise), but where the outlier removal

and smoothing still gave an estimate of the bathymetry. These areas are easy to spot as noise in figure 4.5. By looking at the standard deviation of the data, it is possible that some of the areas could be classified as not bathymetry automatically. However, a good automated process for doing this was not developed in this project. Instead, the areas that were clearly not bathymetry data points were manually removed.

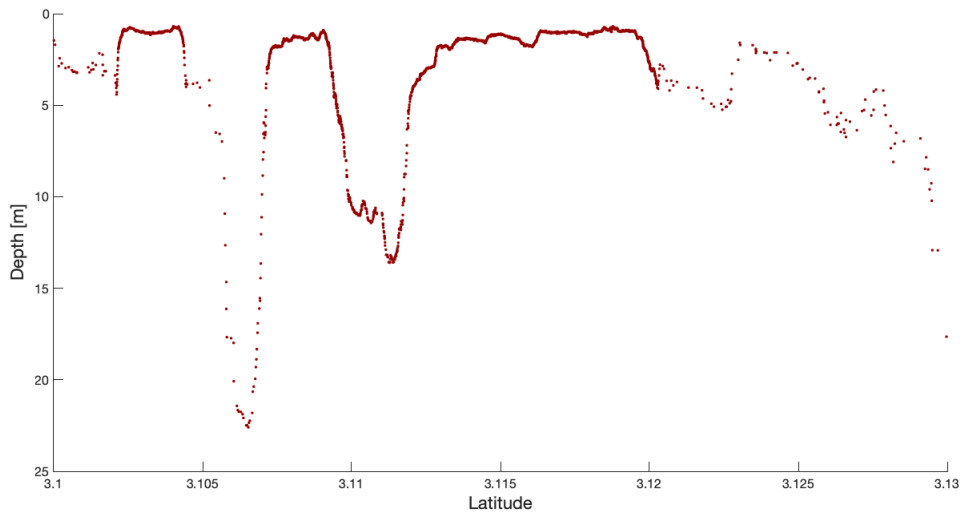


Figure 4.5: Bathymetry profile after data processing (beam GT3R from 2019-09-10)

4.2 Sentinel-2 multi-spectral imagery

Before building a model that can predict water depths based on the multi-spectral images from the Sentinel-2 MSI product, the data first has to go through some pre-processing steps. All pre-processing steps are carried out in SNAP.

1. Resample images
2. Spatial subset and band subset
3. Remove land and cloud pixels
4. Remove sun-glint if needed

After the data has been pre-processed it can be used together with ICESat-2 bathymetry data, to build a linear band model (LBM) for water depth prediction. The model is implemented as an inverse problem in MATLAB using the methods described in section 2.2.2.

4.2.1 Resample images

First, the data has to be resampled. Since the SWIR band, B12, is needed for a land mask, it needs to have the same spatial resolution as the other 3 bands (10 m). Each B12 pixel (20m) is simply slit into four new pixels with the same pixel values as the original pixel. This means that the land mask will not be as detailed, as if we had a SWIR band with 10 m resolution, but it is sufficient for this project.

4.2.2 Subset Images

In figure 4.6 band B02 from the Sentinel-2 scene covering Dhiggaru and Mulah is shown. The full scene is very big, and since we are only interested in the coastal areas around specific islands, a spatial subset was taken. The subsets used for Dhiggaru and Mulah are shown in pink on the figure. Only a few bands (out of the 13 bands available in the Sentinel-2A product) were needed, and therefore only a few bands are saved and used later. The subset is carried out in the SNAP graph builder. The band subset includes B02, B03, B04, B12 and B08.

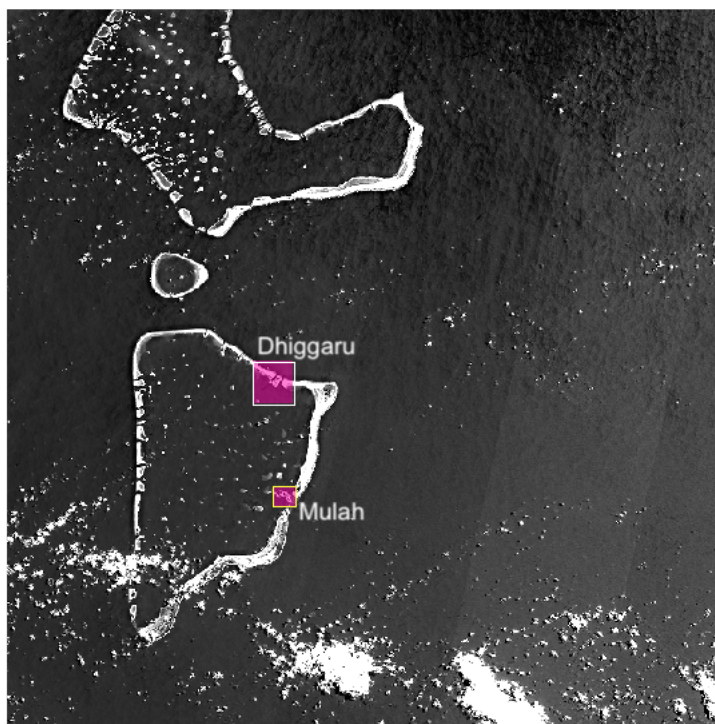


Figure 4.6: Full Sentinel-2 scene (B02) from 2020-08-19, with the Dhiggaru and Mulah subsets in pink.

4.2.3 Land and cloud mask

Once the data is resampled and reduced in size, the land and cloud pixels have to be removed. In figure 3.7d it is clear that land and clouds are easily discernible

in the B12 SWIR band. Since the SWIR band has almost no reflectance in water it is very easy to separate water from land and clouds. In this project, a simple threshold was used. All pixels below a certain threshold was seen as water, and all pixels with values above the threshold was set to NaN. A similar method was used in (Misra et al., 2018).

This successfully removes land mass and also clouds. However, any shadows from clouds are not removed. In figure 3.7d a cloud shadow is visible under the cloud in the upper left corner of the image. The built-in cloud mask from the Sentinel-2 MSI product does not capture small clouds such as the one in the image in figure 3.7d. It is possible to manually mask out the entire cloud, however that would be quite tedious. In this case, the cloud and shadow is not in an area where the model will be trained. Therefore the model itself will not be affected but the water depth estimated within the shadow will be unreliable. The best solution is to find a Sentinel-2 image where the study area is cloud free. An image covering Dhiggaru and Mulah was also found on a different date with no clouds, which is the optimal solution, and the one used to build the final model in this project.

4.2.4 Sun-glint

Sun-glint is the specular reflection of light from the water surface. It will often cause very bright pixel values, especially on rough water surfaces. This can in turn obstruct seafloor features below the water affected by sun-glint. If the seafloor reflection is obscured, it is hard to distinguish different bottom types and to map the bathymetry. The issue is more problematic for high resolution imagery and at shallow waters, where wind blown waves occur easily (Overstreet and Legleiter, 2016).

The intensity of sun-glint depends, among other things, on illumination and viewing geometry. Therefore it is possible to design flight paths to minimize sun-glint. Sun-glint typically forms along wave edges, and can be seen as white bands in figure 4.7, where Buruni is shown in the blue band B02. Buruni is located on the northern side of the Thaa Atoll, which means that north of Buruni we see big open ocean waves. These are not the issue, as they are over optically deep waters, where the seafloor is not visible regardless of sun-glint. It is not clear from the image whether there is a significant amount of sun-glint closer to the island.

The bottom reflectance around Buruni (and the other islands) is very bright, making it hard to see the effect of sun-glint on possible waves.

The issue of sun-glint on shallow water is also a bigger problem with even higher spatial resolution, than the 10 m resolution of the Sentinel-2 bands, since the waves in these areas are smaller than ocean waves. However, depending on the the wind conditions, the angle of the sun and the spatial resolution of the satellite images, sun-glint correction can have a large influence on the ability to see the bottom reflectances.



Figure 4.7: B02 band from 2020-06-30 (Buruni)

(Hedley et al., 2005) presented a simple method for de-glinting the water surface. The method utilises two assumptions: that the NIR band is composed only of sun-glint and a spatially constant component and that there is a linear relationship between the amount of sun-glint in the visible bands and the NIR band. NIR wavelengths (700–1000 nm) are not able to penetrate through deep water, and even in shallow waters NIR has a low water-leaving radiance. This makes the NIR band perfect for sun-glint detection. The de-glinting method can be implemented with the following equation:

$$R'_i = R_i - b_i(R_{NIR} - Min_{NIR}) \quad (4.1)$$

Each pixel value, R_i , in band i can be corrected to a de-glinted pixel value, R'_i . This is done using the NIR band (B08 in Sentinel-2). An area where the reflectance is believed to be constant, if there was no sun-glint, is chosen. A linear regression of NIR pixel values (x-axis) against the optical visible band pixel values (y-axis) is carried out for each band, resulting in a slope, b_i , for the i 'th band. The minimum pixel value in the NIR band in the chosen area is also needed. The difference between the pixel value in the NIR band, R_{NIR} , and the minimum pixel value in NIR, Min_{NIR} , illustrates the amount of sun glint in the given pixel. The slope of the linear regression, b_i , is used to predict the de-glinted value, since it reflects the linear relationship between NIR and the given visible band.

4.3 Combining ICESat-2 and Sentinel-2 for satellite derived bathymetry

After pre-processing we have bathymetry estimates from ICESat-2 data. These water depths will be validated using the single beam data available for the area. The Sentinel-2 image has been reduced in size, and only de-glinted water pixels remain for three optical spectral bands.

A combination of the ICESat-2 estimated depths and the reflectance values in the post-processed Sentinel-2 images will be used in the linear band model. ICESat-2 depths will be used as known depths in the LBM and Sentinel-2 as the multi-spectral imagery. The implementation of the LBM using Sentinel-2 and ICESat-2 will follow the method presented in section 2.2.2. To train the inverse problem, the ICESat-2 depths will all be assigned to the nearest pixel in the Sentinel-2 image. If more than one ICESat-2 data point is assigned to the same pixel, an average depth is found. This is similar to the method used in (Lyzenga et al., 2006).

Just like for the ICESat-2 data, tides should be considered for the Sentinel-2 data. Depending on data acquisition time, the tides might be higher or lower than the MSL. Since one of the inputs in the LBM is known depths, they will define the reference height for the resulting modelled depths. It was tested in this project, whether including information of the local tide at the Sentinel-2 acquisition time would improve the model. However, it did not make any difference on the final result. Therefore it is only important that the ICESat-2 depths in the LBM will determine the reference frame of satellite derived bathymetry.

To sum things up, all ICESat-2 estimated depths are assigned to a pixel, and the corresponding pixel values in each band and the average ICESat-2 depths in each pixel are used to train the model, in order to find the model parameters in \mathbf{m} . This is set up as a system of equations and solved as an inverse problem, using either the least squares method or the damped least squares method. The resulting model parameters can then be used, together with the pixel values in each band, to estimate a depth in each image pixel. This results in a fully satellite derived bathymetric map, using a combination of ICESat-2 and Sentinel-2 data, which will also be validated.

5 Results

5.1 ICESat-2 LIDAR Bathymetry

All tracks covering the three islands were inspected and went through the processing steps described in 4.1. All data points that were not considered to be bathymetry at the end of the processing steps were removed manually.

In order to assess how well the ICESat-2 LIDAR measures seafloor depths, the results are validated using single beam measurements from the area around each islands. The validation data was first interpolated to a grid, and then to the center coordinates of the ICESat-2 data points. Only ICESat-2 points that were within 8 meters of a single beam measurement were included in the validation. If the nearest validation data point is far away, the interpolated value is more likely to be incorrect, and therefore a limit was imposed. Since the ICESat-2 footprint is 17 meter in diameter, the 8 meter distance between ICESat-2 and single beam data point will ensure some overlap, and hopefully reduce the error introduced by the interpolation. The data point positions might also have horizontal errors, however any inaccuracies in the coordinate precision was not considered when deciding which data points to use for the validation.

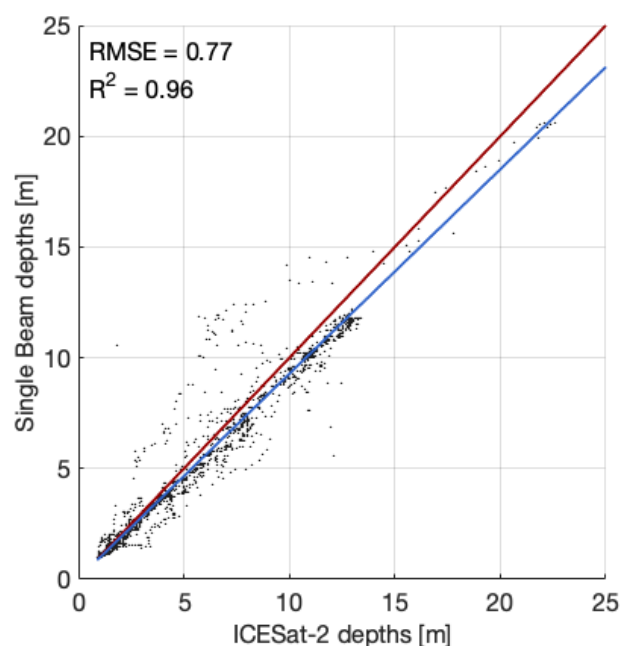


Figure 5.1: ICESat-2 estimated depth vs single beam depths (Dhiggaru). The red line represents a 1:1 linear line, while the blue is a regression line.

Figures 5.1 and 5.2 show the correlation between the depths estimated by ICESat-2 and the depths estimated by the single beam measurement. The single beam depths are the best estimate we have of the actual depths in the area. The red line represents a 1:1 linear line, while the blue is fitted to the data. For Dhiggaru we see a good linear correlation with an R^2 value of 0.96 and a RMSE of 0.76 m. Additionally we see that there are many measurements in the 0-15 meter range and only a few between 15-25 meter. The deepest measurement is 22.6 meters. While the correlation between the data points (especially between 0-15 meters depth) is close to linear, there is a small bias for the ICESat-2 estimated depths to be deeper than the single beam depths.

There are some data points above the blue line, where the residuals are fairly large, and where ICESat-2 has underestimated the depths. These errors are most likely from steep areas of the bathymetry, where large errors occur more easily, as it is hard to capture a sudden change in depth. This will be explored further in a visual analysis of the bathymetry in section 5.1.1.

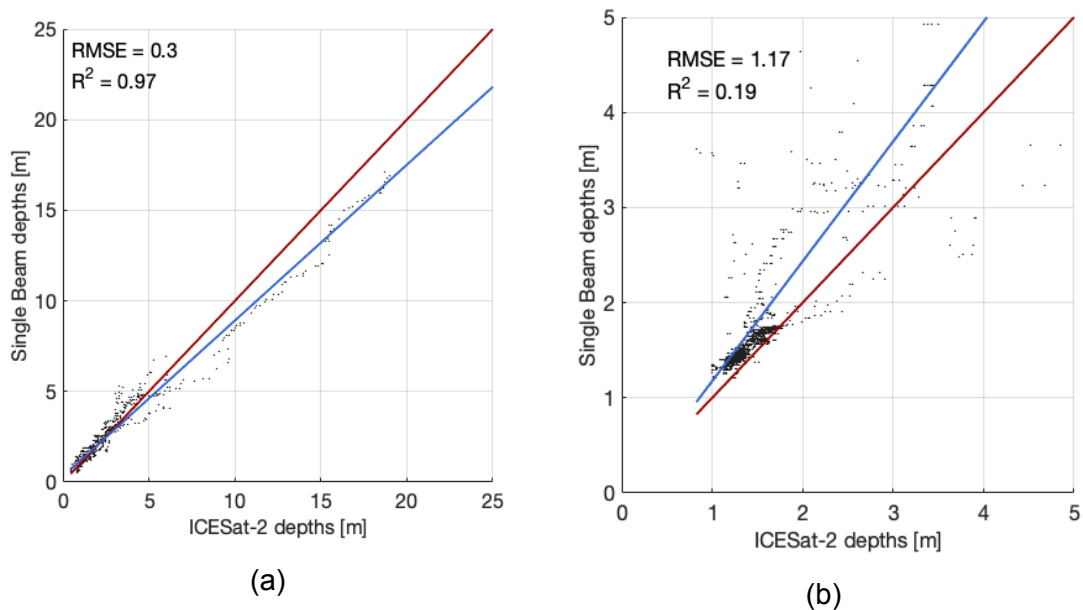


Figure 5.2: ICESat-2 estimated depth vs single beam depths a) Buruni b) Mulah. The red line represents a 1:1 linear line, while the blue is a regression line.

In figure 5.2 the correlation between ICESat-2 and single beam depths for Buruni and Mulah are also shown. For Buruni there is a good linear correlation with an R^2 value of 0.97 and the RMSE is 0.3 m, which is smaller than RMSE for the data around Dhiggaru. From 5.2a it is also evident that there are fewer large residuals, resulting in a smaller RMSE. However, there are also fewer deep measurements,

and the largest concentration of points are between 0-5 m. The deepest measured depth in the water around Buruni is 19.7 m. The results of the ICESat-2 bathymetry around Mulah is the least successful. It is apparent in 5.2b, that there is a poor correlation between ICESat-2 and single beam estimated depths. Between 1-2 meters depth there is a larger concentration of measurements with a decent, close to linear, correlation. However most measurements deeper than 2 meters show no correlation. This is reflected in the low R^2 value of only 0.19, and the larger RMSE of 1.17 m. These values are even poorer considering the measured ICESat-2 depths are only between 1-5 meters deep. While Dhiggaru and Buruni have a RMSE of 3.5% and 1.5% of the maximum depth, Mulah has a RMSE of 23% of the maximum depth. A visual inspection of the area and a few selected tracks will shed some light on difficulty of mapping this area.

In (Parrish et al., 2019) the ICESat-2 bathymetry was estimated to have a RMSE of 0.43-0.60 m, with a maximum depth of 38 m, resulting in a RMSE of 1.6% of the maximum depth. While it is based on data with a deeper maximum depth and validated using airborne LIDAR, it indicates the same accuracy as seen for Dhiggaru and Buruni, where the RMSE is 1.5-3.5% of the maximum depth. They also found the maximum penetration depth to be 0.96 Secchi depths. We do not know the precise Secchi depth for the water around these islands, but the penetration depth of 22.6 and 19.7 meters for Dhiggaru and Buruni is probably around 0.66 - 1 Secchi depths (assuming a Secchi depth of 20-30 meters).

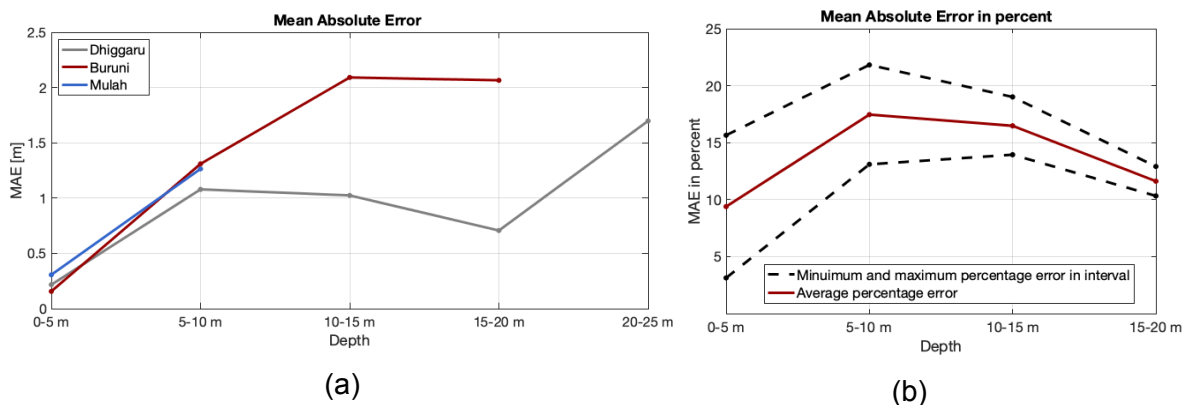


Figure 5.3: a) MAE of ICESat-2 estimated depth vs "true depths" (single beam) for all three islands at different depths. b) Percentage MAE for Buruni.

An analysis of the error with increasing depth was also carried out. In figure 5.3a the mean absolute error (MAE) at increasing depths is shown for all three islands.

The MAE is generally low in the 0-5 meter interval, with values ranging from 0.15 m to 0.3 m. The MAE increases with increasing depth, with the lowest errors seen for the ICESat-2 data around Dhiggaru. In the deeper water 15-25 meters, the MAE is around 2 m for both Dhiggaru and Buruni. This is still acceptable, as it is expected that the accuracy declines with depth. The same is expected for single beam measurements, so the higher error at greater depths can also be partly due to an error in the validation data. When looking at the error as a percentage of the depth, we see that the average error is between 3-20 percent for ICESat-2 bathymetry measurements around Buruni.

5.1.1 Visual Inspection of ICESat-2 bathymetry

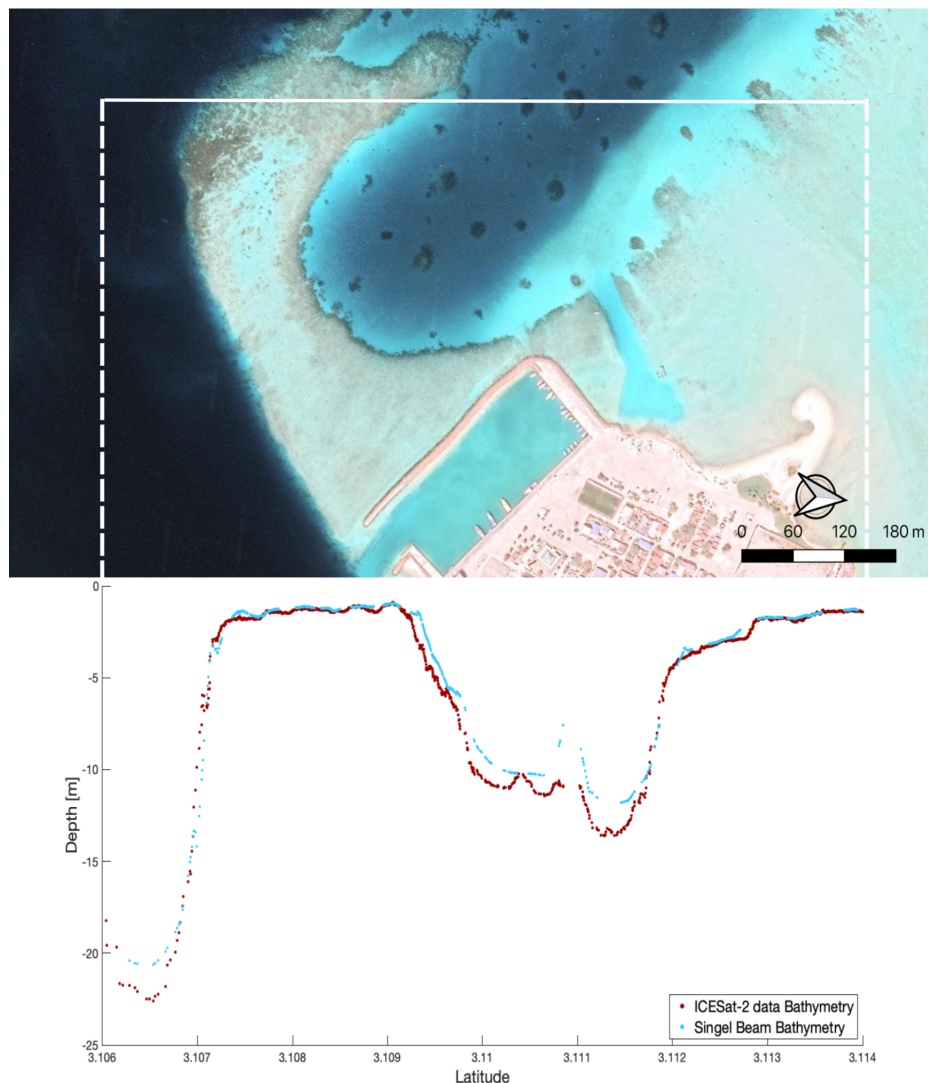


Figure 5.4: ICESat-2 bathymetry in red and single beam bathymetry in blue. The white line across the satellite image shows where the bathymetry profile is from (Dhiggaru). (ICESat-2 beam GT3R from 2019-09-10)

Visual inspection can also shine a light on some validation issues and the limitations of ICESat-2 bathymetry.

In figure 5.4 the result from a single ICESat-2 track is shown in parallel with the position of the track on a satellite image. The track crosses near the island Dhiggaru, across the coral reefs surrounding the island. The bottom part of figure 5.4 shows a bathymetry profile along the track, the red points are ICESat-2 points after the processing described in section 4.1, and is actually the same profile as shown in figure 4.5. Here we only look at the part of the bathymetry where ICESat-2 and the verification data (single beam data) overlap. The single beam data has been interpolated to the same coordinates as the ICESat-2 point coordinates for easy comparison. There are gaps in the single beam profile, since only the data used for validation is included. Gaps in the data indicate that the nearest single beam data point was too far away, for the comparison to make sense. Generally it is clear to see that the two bathymetry profiles follow each other well, especially in the more shallow water. There is a tendency for ICESat-2 to measure the seafloor as deeper than the single beam measurements, which is more evident in the deep water.

There is an obvious problem between 3.11 and 3.12 degrees north. When looking at the satellite image in the top part of figure 5.4, we see that the track crosses two coral heads. In the ICESat-2 bathymetry, there are two small bumps that clearly correlate to the coral heads. In the single beam data, only one of these coral heads are visible. Since the ICESat-2 footprint is 17 meters in diameter, it might measure the coral head in the edges of the footprint. The single beam data is interpolated to the center coordinate of the footprint, so while the single beam measurements might have captured the coral head, it might simply be an interpolation error. Or, perhaps the single beam did not cross this coral head. None the less, for the coral head that is visible, the single beam method is able to discern the top of the coral head as much more shallow than ICESat-2. When looking at the original ICESat-2 data (also shown in figure 4.4), there is an indication that the top of the coral head is measured. However, it is hard to distinguish from noise, and it has been removed in the data processing.

There is a very steep area around 3.107 degrees north. Visually, the two bathymetry methods follow each well, but the steep area introduces errors in the validation. This is because a slight horizontal misalignment causes large vertical errors when the area is this steep. The data points that are being compared all have the same coordinate, but they appear to be up to 10 meters apart vertically. This is hard to

account for in the validation, however it is important to note that some of the larger errors seen in figure 5.1 are probably due to this rapid depth change, where both single beam and ICESat-2 clearly captures the steep descent, but the interpolation and small inaccuracies in coordinate position can contribute to a larger error, than what is actually applicable.

At the deepest point in the bathymetry profile in figure 5.4, there is a gap between the ICESat-2 bathymetry and single beam bathymetry. They follow the same curve, but the two methods disagree on the actual depth. What causes this difference is hard to say, as the accuracy simply is worse at greater depths. It can be an imperfect refraction correction, however the error can also be from inaccuracies in the single beam acquisition.

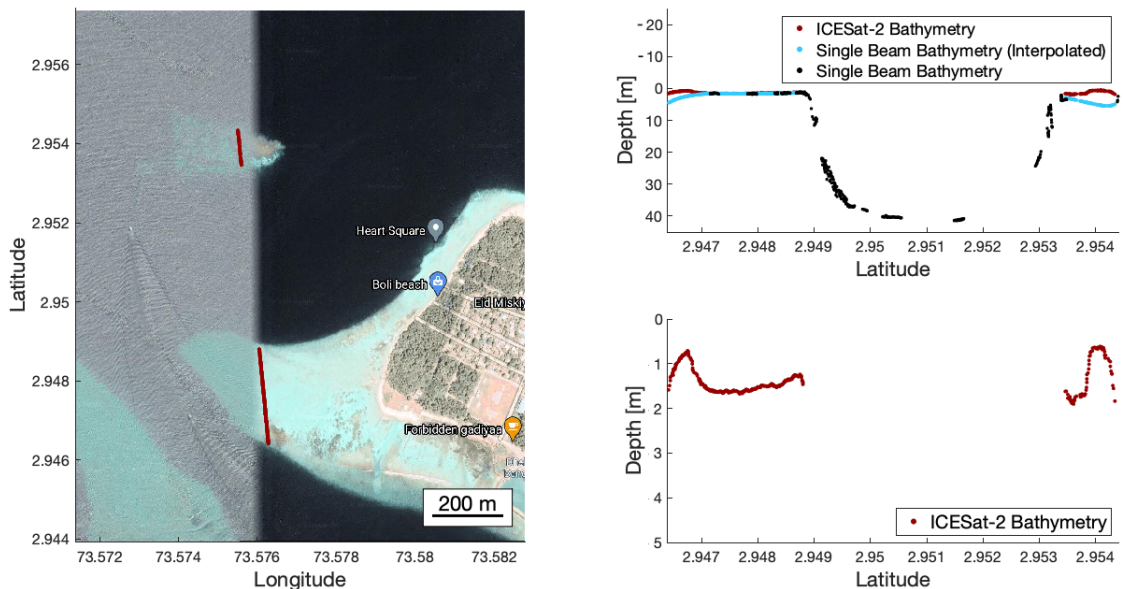


Figure 5.5: Beam track crossing the coral reef surrounding Mulah. Track shown on satellite image (left). The profile showing the single beam depth (before and after interpolation) and ICESat-2 depth. (top right). Just the ICESat-2 depths (bottom right) (Beam GT3L from 2019-09-10)

Just like the steep slope mentioned above in 5.4, steep slopes are also a challenge around Mulah. In figure 5.5 an ICESat-2 beam track is shown to cross the coral reef west of Mulah. In the satellite image, the red line shows the area where bathymetry was estimated. The dark water between the bright coral reef was too deep for any depth estimates from ICESat-2. The depth estimate from ICESat-2 is shown in the bottom right bathymetry profile in figure 5.5, where we see that the depths are around 1-2 meters. The same depths are shown in the pro-

file above, where the single beam depths are also shown. The blue points show the single beam data interpolated to the same location as all the red ICESat-2 data points. The black single beam depths show all the single beam data points that fall on the line along and between the ICESat-2 beam track. The blue interpolated depths give us an insight in the interpolation limitation. Both the far left side of the bathymetry and the right side of the bathymetry profile show large differences between single beam and ICESat-2 depths. However, we also see that the black data points, which are the single beam data before interpolation, are not close to the interpolated points. It is also possible to see in figure 3.8b, where the single beam track is shown, that the single beam data does not cover the smaller coral reef, where the ICESat-2 track crosses at 2.954 degrees north. The boat collecting the single beam data probably did not want to cross this area, as it is so shallow it could impose a risk to sail across. This illustrates the importance of satellite or airborne data, however it also means that we are not able to validate the depths in this area. In the validation, only data points with a single beam data point within 8 meters were used, so most of the ICESat-2 depths in the far left and right in the bathymetry profiles are not included in the validation.

In between the two areas measured by ICESat-2 we know the depth because the single beam was able to measure the depths in the area. From the top right bathymetry profile in 5.5 we see that the depth drops from 2 meters to 40 meters very rapidly. The steep slope is not captured by ICESat-2, however the very edges of the coral reef is. Again a small error in the horizontal position might result in large errors in the vertical.

The deepest measured ICESat-2 depth is 38 meters in the (Parrish et al., 2019) study. This makes the seafloor around Mulah hard to map using ICESat-2. The shallow coral reef is easy to identify, however the steep descent to deep waters, and the generally deep seafloor outside the coral reef makes it very hard for ICESat-2 LIDAR to measure.

There is however an indication that ICESat-2 is able to penetrate far into the water. In figure 5.6 we see the bathymetry profile of ICESat-2 beam GT3R from 2019-09-1 as it crosses west of Mulah. The top profile shows the tide and refraction corrected data, but without outlier removal as dark blue. The light blue in both profiles shows the single beams data that falls on the same line as the beam track (not interpolated). The red data points in the bottom profile is the ICESat-2 depths after outlier removal and smoothing. In the red box we see something interesting. Along the seafloor measured by single beam, there is a line of ICESat-2 data

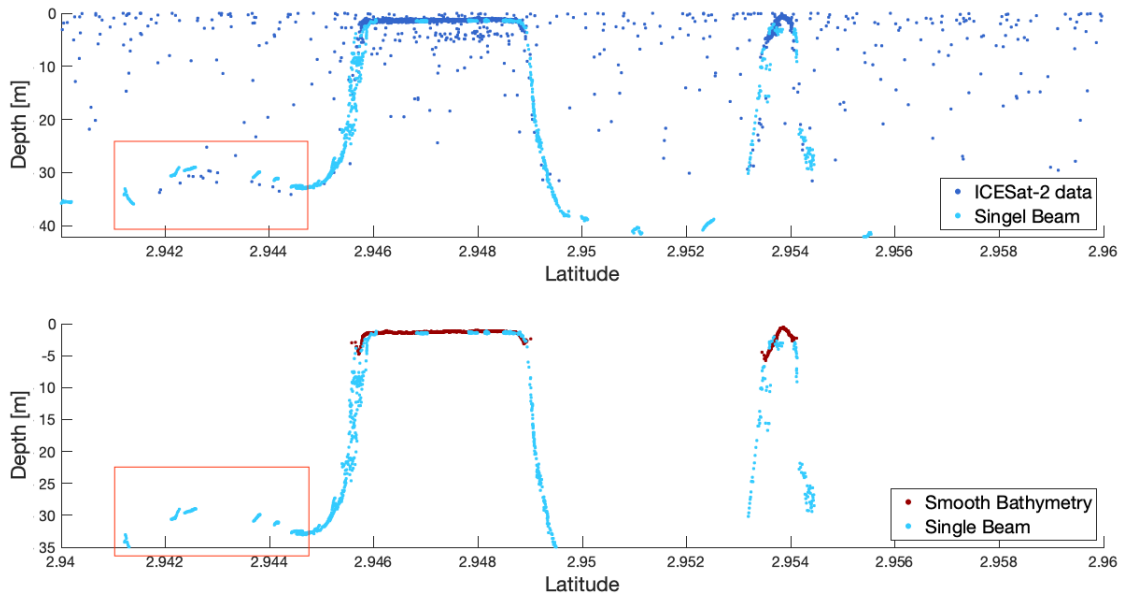


Figure 5.6: Bathymetry profile showing ICESat-2 data from 2019-09-10 (beam GT3R). The tide and and refraction corrected ICESat-2 data shown in blue in the top profile, and the same data after outlier removal and smoothing as red in the bottom profile. The light blue data shows single beam depths.

points, that follow the same seafloor curvature as single beam has measured. This is at around 30 meters depth, indicating a good water penetrating ability. However, had we not had the single beam data in the same figure, this would probably be categorized as noise even with visual inspection. It is therefore no surprise that the outlier removal method used in the project has removed these data points. This illustrates that even if the ICESat-2 LIDAR might measure the seafloor, it can at times be indistinguishable from the background noise.

5.2 Combined Sentinel-2 & ICESat-2 Satellite Derived Bathymetry

This section will go through the process of choosing the most optimal model and discuss the parameters that were considered. The optimized model will then be validated at all three islands using single beam data, while discussing factors that can induce larger errors, and what is needed for a successful bathymetry model. Finally, the model will also be validated in a case where the single beam data is used to train the model instead of using ICESat-2 data.

5.2.1 Optimizing Satellite Derived Bathymetry Model

In order to optimize the model, different variations of the data input and parameters have been tested.

The variable X_j described in section 2.2 can be defined in different ways. In (Ma et al., 2020) it is unclear how they define X_j , but it appears to simply be the reflectance value in the j 'th band of the Sentinel-2 image. However, most other implementations of the linear band model use the log of the reflectances. In figure 5.7 the RMSE at increasing depths are shown, with X_j as just the reflectances and with X_j as described in equation 2.18 where the log of the reflectances are used. The RMSE is based on the multi-spectral Sentinel-2 bathymetry model of Dhiggaru validated using the single beam data. It is clear that the model with the log of reflectances is much better.

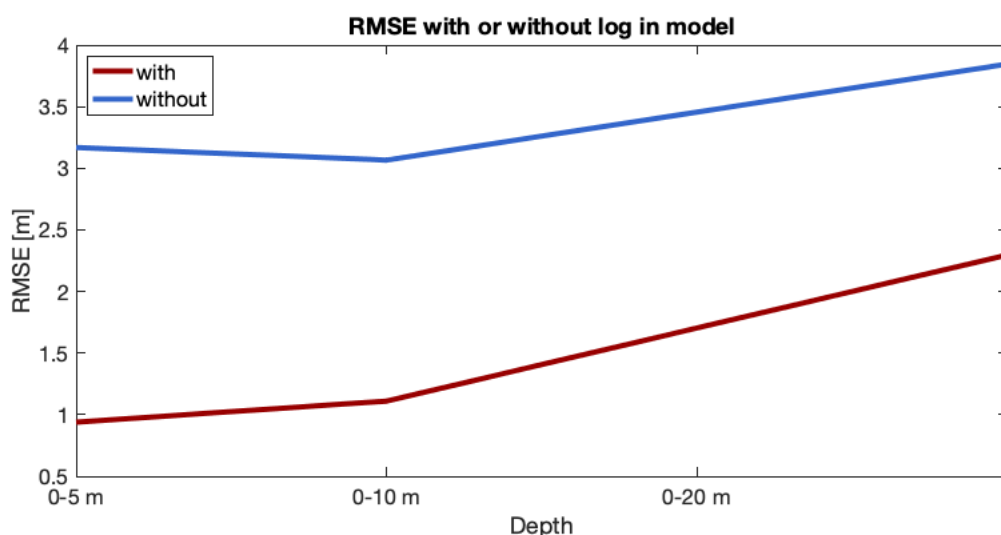


Figure 5.7: RMSE at different depth intervals with or without logarithm in model (Dhiggaru)

In order to train and build the model, an inverse problem was formulated. The

model parameters used to build the model, was found using both a least squares method and a damped least squares method. In figure 5.8 we see that the RMSE at different depths varies very little between the two methods. Since it is easier to implement the normal least squares, this will be used.

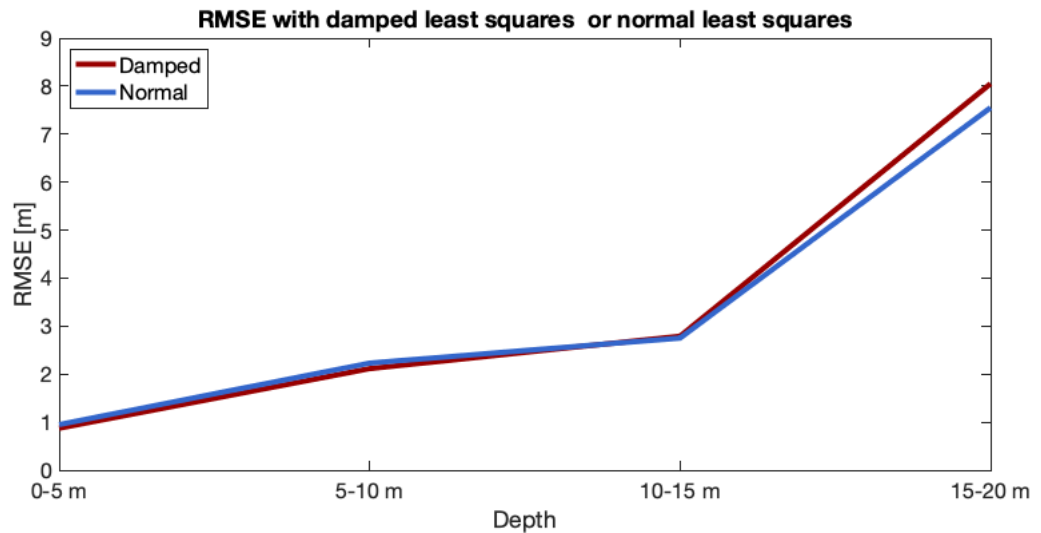


Figure 5.8: RMSE at different depth intervals with damped least squares or normal least squares (Dhiggaru)

Another idea for how the model could be improved, was to distribute the model input depths, such that there were an equal amount of data points at all depths. The input depths from ICESat-2 are over represented in the shallow end, especially between 1-3 meters. Since the model tries to fit as many data points as possible, the model will end up with only few deep areas, and possibly not fitted to the deepest input points. So even though there are ICESat-2 data points down to 22 meters for Dhigarru, the maximum depths in the multi-spectral model is around 20 meters. To try and account for this, the ICESat-2 depths were redistributed, such that the depths were more evenly distributed at all depths between 1-22 meters. Figure 5.9 shows the RMSE at different depths with or without redistributing the input depths. When redistributing the depths more evenly, the RMSE does decrease in the 15-20 meter interval, however there is a small increase in RMSE in the 0-5 meter interval. This is as expected, since the model should try to fit to both the shallow and deep depths, instead of mostly fitting to shallow depths. The difference is not big, however it is still noticeable especially in the deep end. This also demonstrates that having a large amount of input data is not necessarily an improvement. There is approximately 90% fewer data points as input with even distribution of depths than without. Despite this, the model still performs al-

most as good in the 0-10 meter depths and even better in 10-20 meter interval. Therefore it is more important to have a wide variety of depths in the area than to have many data points at the same depth.

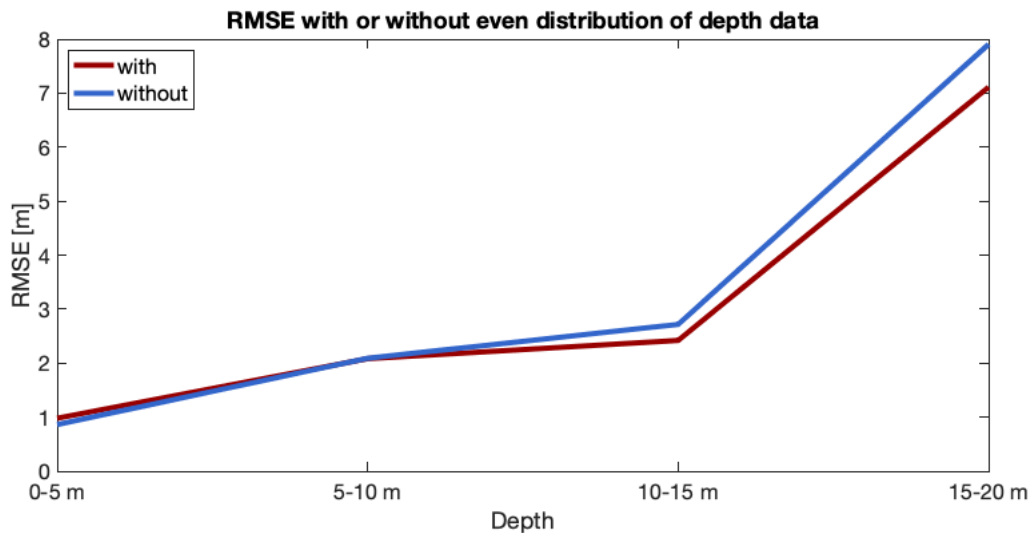


Figure 5.9: RMSE at different depth intervals with or without even distribution of depths as input in model (Dhiggaru)

Finally, a test was carried out in order to see if de-glinting the Sentinel-2 image would improve the multi-spectral bathymetry results. The de-glinting was carried out as described in section 4.2.4, and a comparison of the RMSE of the resulting modelled bathymetry with or without a de-glinted image as input is shown in figure 5.10. Again we see only a small difference in the RMSE between the models with the two different inputs. However, this is possibly due to a small amount of sun-glint in the image over shallow water, and not necessarily because the de-glinting method does not work. The sun-glint was not easily discernible in the shallow waters around the 3 islands, but in areas where sun-glint is a bigger issue it could be important to use de-glinted images in the model.

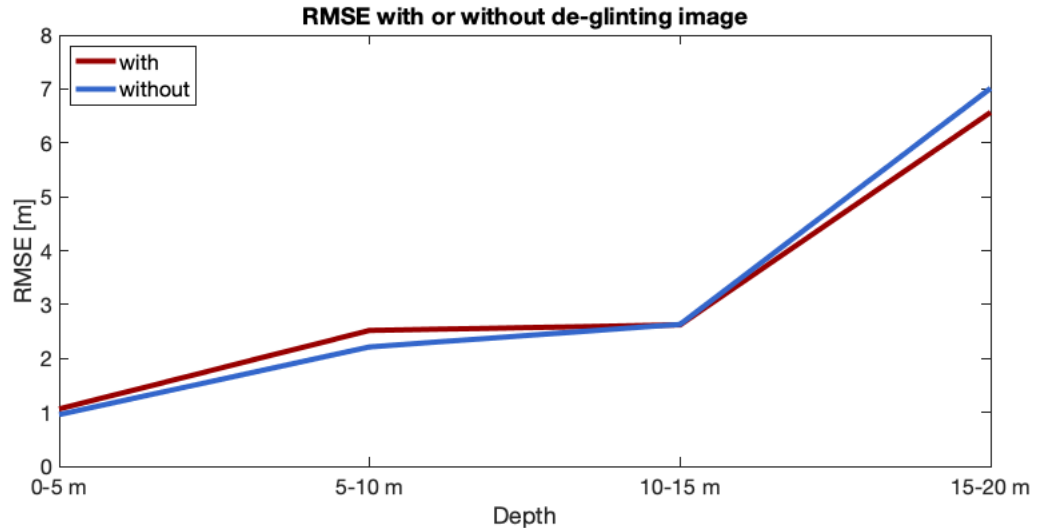


Figure 5.10: RMSE at different depth intervals with or without de-glinting image bands for input in model (Dhiggaru)

5.2.2 Validating final Satellite Derived Bathymetry model

The optimal parameters and inputs based on the previous section is used for all validation of the model going forward. The logarithm of the reflectances, the normal least squares, even distribution of depth in the input depth data and Sentinel-2 image without de-glinting is used.

This resulted in three modelled depth maps, one for each island. They can be seen in figure 5.11. Each map covers the full extent of the Sentinel-2 image subset that was chosen. For Dhiggaru, the extent covers an area further away from the island than for the other two islands. However, since the single beam data used for validation is only available close to the islands, the size of the covered area does not affect the validation.

It is apparent from the modelled depth maps, that the areas closer to the islands are more shallow, and further away from the island the water becomes deeper. This is of course no surprise, however only a little knowledge of the area is needed to know that the areas further away from the islands are most likely deeper than seen in the models. The water north of Dhiggaru in figure 5.11a is estimated to be ~20 meters deep, which is unrealistic since it is open ocean, outside the atoll. The water here, and possibly much of the water in these maps, is optically deep, meaning that the seafloor is not visible, and the model has no chance of estimating the correct depth. It is possible to remove optically deep pixels, but it was chosen to keep all the pixels for validation.

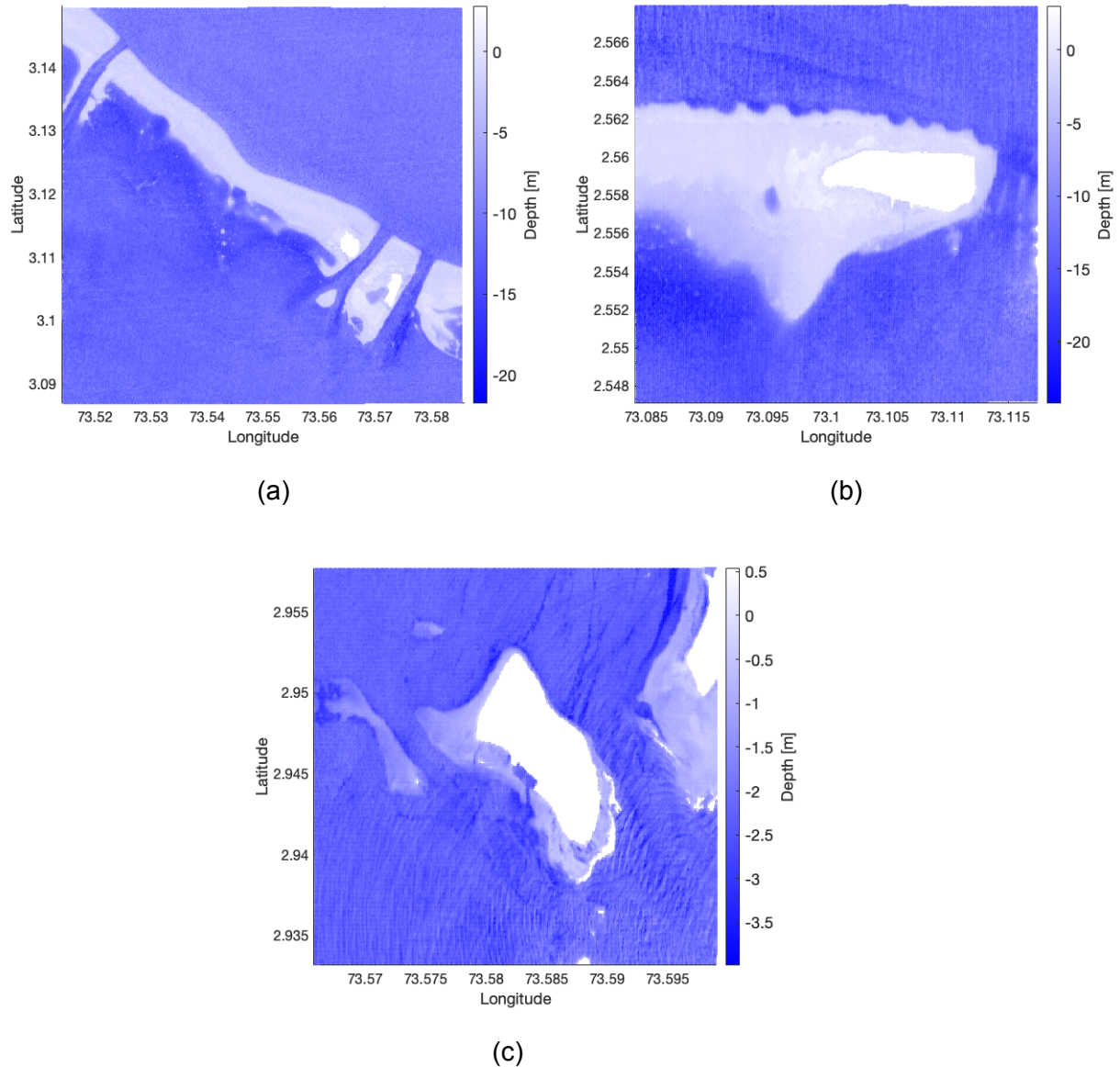


Figure 5.11: Modelled depths for a) Dhiggaru b) Buruni and c) Mulah

For both Dhiggaru and Buruni, figure 5.11 a and b, the modelled depths are estimated to be down to ~20 meters depth. However, there are also some areas that are estimated to be above the sea level. Some of the areas estimated to be above sea level were dark in the satellite image, meaning that it is likely a different bottom type that is harder to map. These areas are small, and given that they are not estimated as water depths, they can be classified as "depth not known". For now they are still kept in the model. The validation was also carried out without these values, but it did not affect the statistical analysis.

When looking at the modelled map for Mulah, in figure 5.11c, it is clear that it has

not been as successful as for the two other islands. The depths are only estimated down to 4 meters, however it is likely that the areas far from the island are much deeper than this. Even before validating the model results, it is clear that there are limitations to the multi-spectral bathymetry method, however we also see that the model has clearly captured some depth variations around the islands.

The modelled depths have been validated using the single beam depth measurements from around the three islands. Similar to the ICESat-2 bathymetry validation, only modelled depths within a certain distance of a single beam data point are used in the validation. This is done because the single beam data is interpolated to the coordinates of the modelled depths, and if there is no single beam data near the modelled data point, the interpolation will not be accurate.

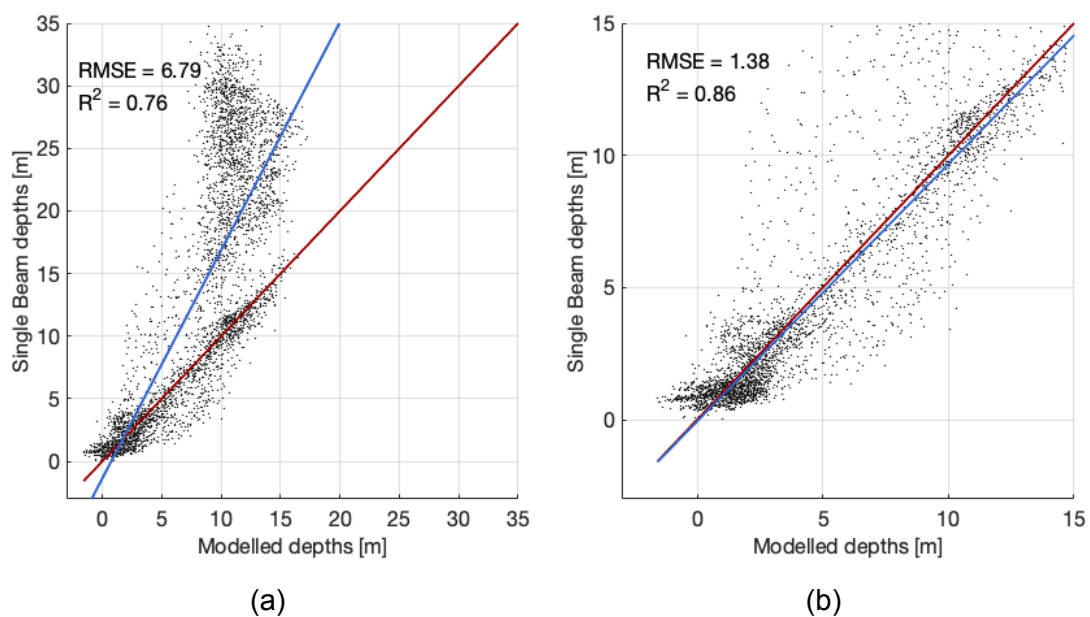


Figure 5.12: Modelled depths vs single beam depths for Dhiggaru. a) single beam depths between 0-35 m b) single beam depths between 0-15 m. The red line represents a 1:1 linear line, while the blue is a regression line.

The interpolated single beam depths are compared to the modelled depths in figure 5.12 for Dhiggaru. The validation is carried out with all single beam data between 0-35 meters depth being compared to the corresponding modelled depth in a, and with only single beam depths between 0-15 meters depth in b. The red line in the two figures is a reference line indicating a 1:1 correlation. The blue lines are linear fits, with a corresponding R^2 value. In the figure 5.12a, it is very

clear that the data does not follow a perfect linear correlation. The blue fitted line is far from the red 1:1 line, and the R^2 value is 0.76, indicating a slightly poor fit. Visually, it is obvious that between 0-15 meters there are a lot of points that fall on the red line. Above 15 meters in the single beam data, the correlation is non-existing. The areas measured to be between 15-35 meters deep by the single beam method are modelled to be 10-15 meters deep by the multi-spectral bathymetry method.

However, when looking at the correlation between the single beam and modelled depths in figure 5.12b, there is a good fit with the R^2 value being 0.86. The RMSE when only looking at depths between 0-15 meters is 1.38 m, much better than the 6.79 m RMSE we see when looking at 0-35 meters. The fitted blue line is also very close to the 1:1 red line, indicating a close to linear fit. While the majority of points follow close to the 1:1 line, there are still outliers both above and below the fitted line, that contribute to large errors.

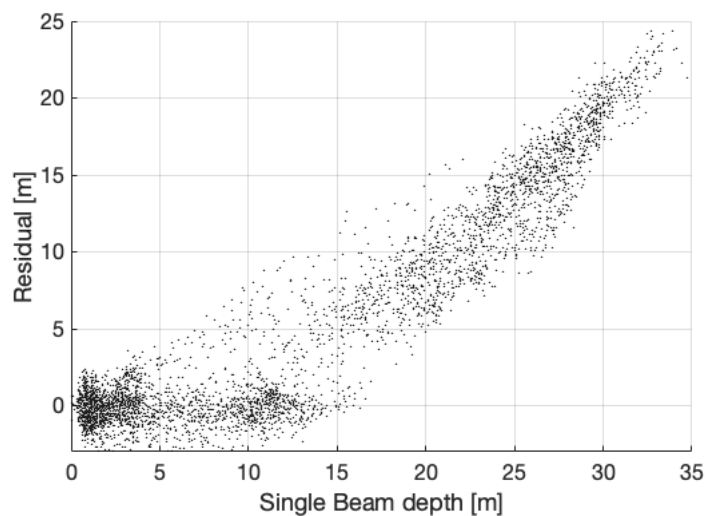


Figure 5.13: residual between modelled depth and single beam depths as a function of single beam depths (Dhiggaru)

Figure 5.13 shows the residual between the modelled depths and single beam depth for each single beam depth. Again we clearly see that the residuals increase around 15 meters depth. The model is built using ICESat-2 bathymetry data, which results in limited depth estimates. Since there were only few data points at depths below 15 meters, it is more challenging for the model to estimate deeper areas correctly. This is even more evident when looking at the results from Mulah, where the input data from ICESat-2 was between 0-5.5 m, with the major-

ity of the data points between 1-2 meters depth. This results in the multi-spectral modelled depths compared to single beam depths seen in 5.14c. There is a poor correlation, which is also apparent in the R^2 of 0.7 and RMSE of 0.96 m, based only on depths between 0-5 meters. Visually, it is also clear that the expected linear correlation is only evident between ~0-2 m.

For Buruni, in figure 5.12a and b, we see a result similar to the modelled bathymetry around Dhiggaru. The correlation between the modelled depth and single beam depths is fairly good down to 15 meters, where the fitted blue line and the 1:1 linear red line are close together and the RMSE is around 1.19 m, and R^2 is 0.83. When the model tries to estimate areas that the single beam has measured to be deeper than 15 meters, the model starts to fail, and the deepest modelled depths are only around 17 m.

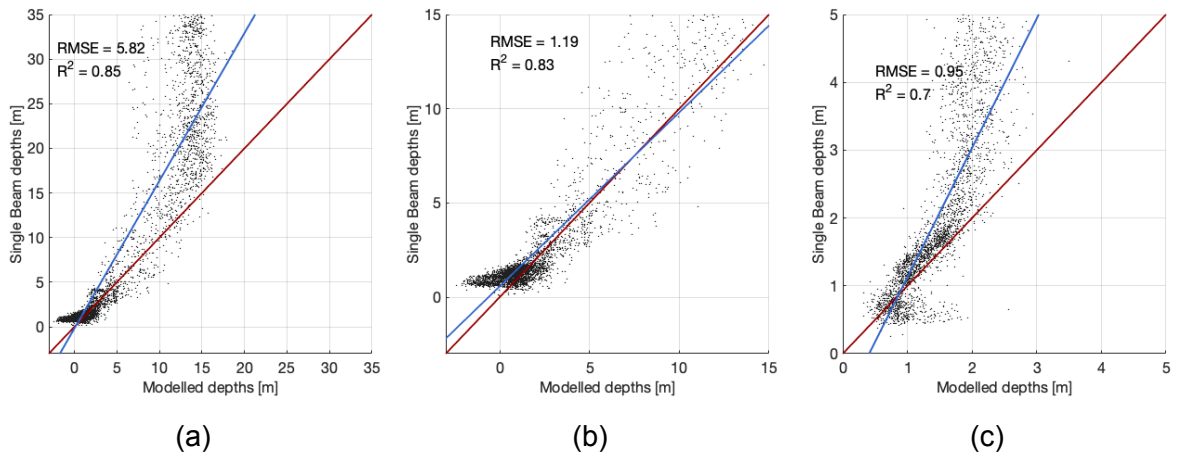


Figure 5.14: Modelled depths vs single beam depths. a) Buruni: depths between 0-35 m b) Buruni: depths between 0-15 m c) Mulah: depth between 0-5 m. The red line represents a 1:1 linear line, while the blue is a regression line.

In figure 5.15 the modelled depths are shown for the area around Dhiggaru where the single beam data is also available. In figure 5.16 the residual are shown for the same area. The model and residual maps make it possible to carry out a visual inspection and discover which areas are most problematic, when estimating depths. In the model map we see that the shallow coral heads that ICESat-2 also captured in figure 5.4, are visible in the western corner of the image. There are small areas with more shallow depths than the surroundings. When looking at the same area in the residual map, it is also clear that the coral heads have not introduced significantly large errors. As expected, the more shallow areas with depths in the interval 0-5 meters have the smallest residuals. The largest resid-

uals are found in the deeper area east of the island. The channel between the two coral reefs, the Dhiggaru Kandu, is hard to map for the multi-spectral method. The area is as deep as 35 meters in some places, making it optically deep for the multi-spectral Sentinel-2 image. This also explains the large residuals. As seen previously, all deep areas are estimated at around 15-18 meters depth, even if they are much deeper. This limitation results in the large residuals in the areas deeper than 20 meters. By identifying the optically deep pixels, it would be possible to separate the areas where the model is likely to correctly have estimated the depths to be ~15 meters, and the optically deep areas that should be categorized as deeper than 15 meters.

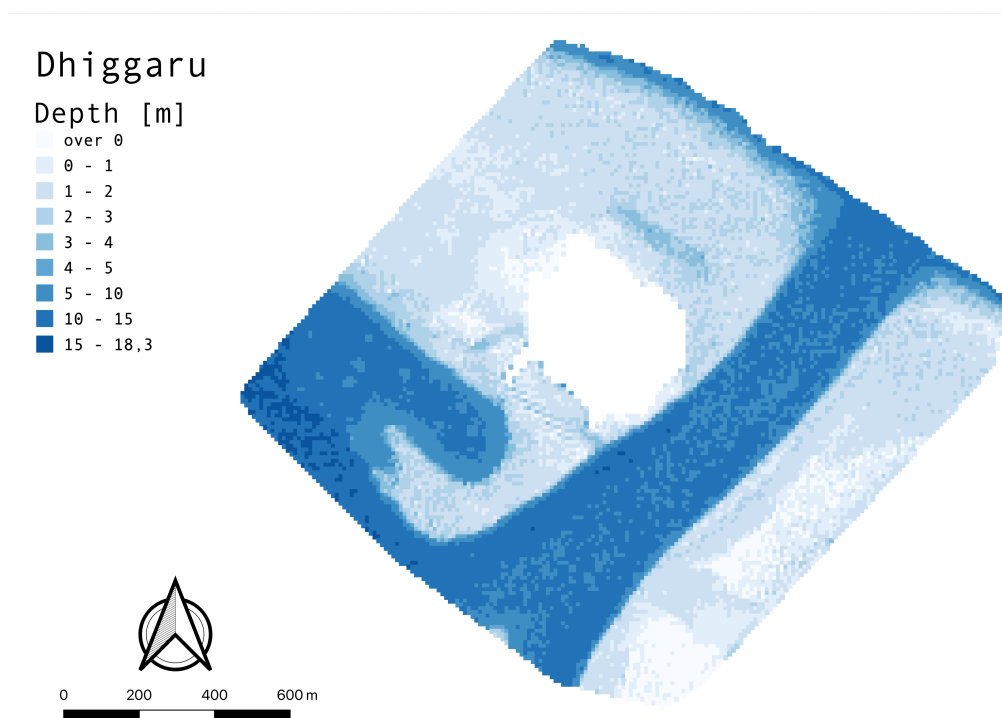


Figure 5.15: Model Map of Dhiggaru in area where there is overlap with single beam data

In (Ma et al., 2020), they also developed a method for processing ICESat-2 data and combining ICESat-2 estimated depths with Sentinel-2 imagery using the linear band model, in order to estimate a satellite derived bathymetry. The study was carried out for shallow water around atolls in the South China Sea and validated using airborne LIDAR. For depths between 0-18 meters they compared the modelled depths with the airborne LIDAR depths with imagery from 4 different dates. This resulted in R^2 values between 0.89-0.93 and a RMSE between 1.25-1.61 meters. These R^2 values are slightly better than what is seen for Dhiggaru and Buruni. However, the RMSE is in the same interval or lower for Dhiggaru and

Buruni. Generally the result and estimated errors are very similar when comparing the (Ma et al., 2020) study with the results of this project. They conclude that the RMSE is lower or or close to 10% of the maximum depth. For Dhiggaru and Buruni the RMSE is 9.2% and 7.9% of the maximum depth (15 meters).

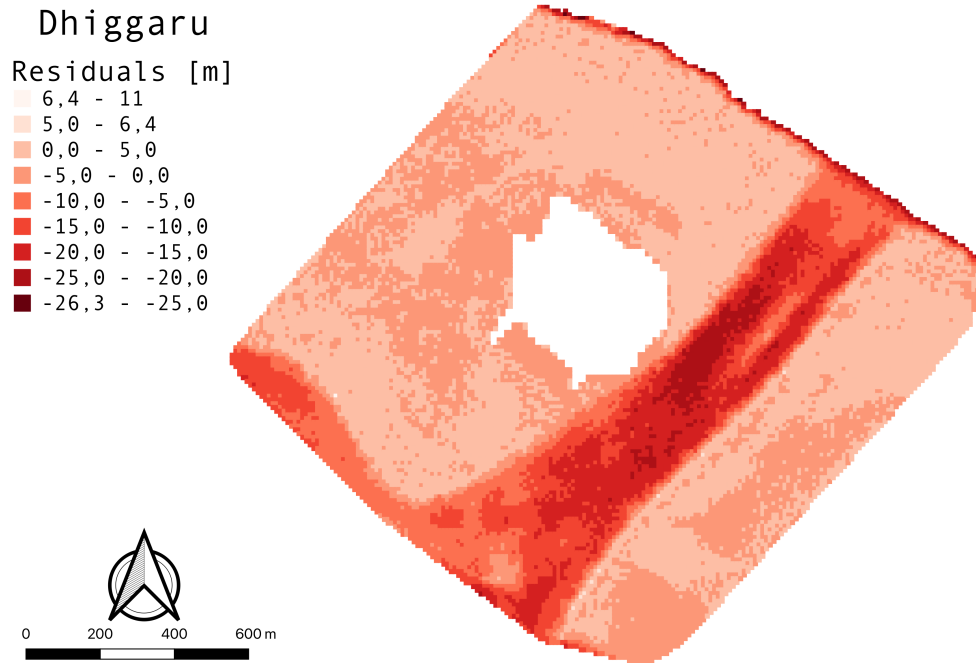


Figure 5.16: Residual Map of Dhiggaru. The residuals are the difference between modelled depths and single beam depths.

5.2.3 Single Beam as input in Linear Band Model

Another way of testing the model, is to use the single beam bathymetry data as input in the model instead of ICESat-2 data. The single beam data is spread out in the entire area around the islands with depths all the way down to 70 meters. The single beam data was split into two equal data sets; training data for input in the model and testing data used for validation.

The model was trained and build three time, once with single beam data between 0-25 meters and once with all the data between 0-70 meters. This is done for Dhiggaru to test whether the model is improved by having more input data, and also with single beam training data between 0-25 meters for Mulah.

In figure 5.17 we see the correlation between the model built on single beam training data between 0-70 meters depths and the single beam testing data. The same correlation, with only training data between 0-25 meters depth is shown in figure 5.18. Just like with ICESat-2 as input in the model, there is a limitation of

how deep the model can estimate depths. In figure 5.17, the model estimates depths deeper than 30 meters. In the deeper end, the correlation between the model and single beam depths is not as poor as it was when ICESat-2 was used as input. However when looking at figure 5.17b, where the correlation is only shown for single beam depths between 0-15 meters, it is clear that the correlation in the shallow end is not good. The model is trained using depths between 0-70 meters, making it hard for the model to fit well in both the deep and shallow end. This has resulted in an RMSE of 3.77 and an R^2 of 0.57. This is much worse than the results in the 0-15 meter interval when ICESat-2 depths were used to train the model.

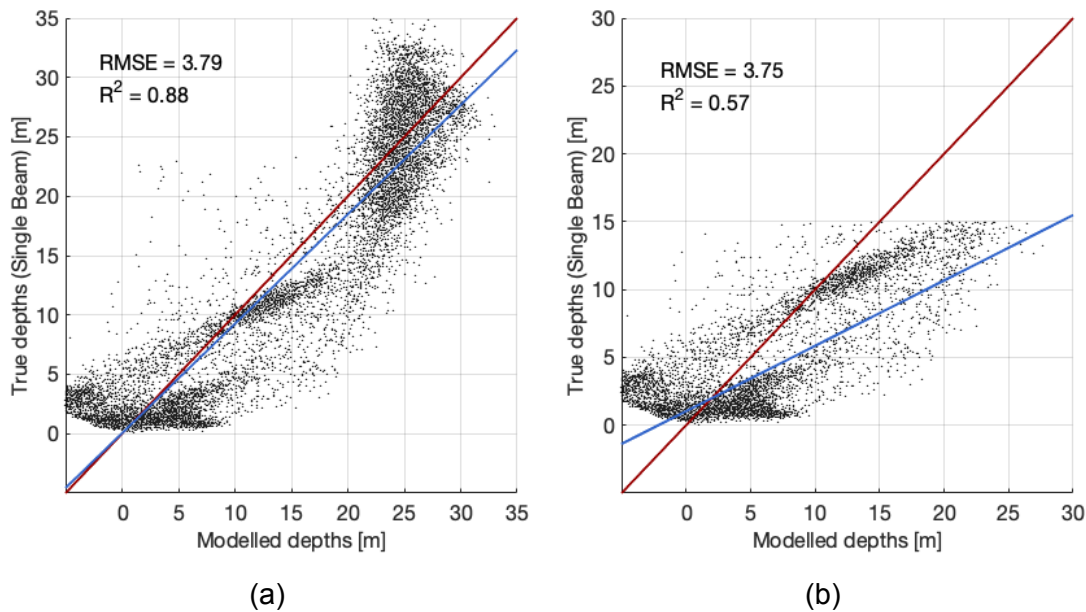


Figure 5.17: Dhiggaru: Single beam depths (0-70 meters) as model input. Resulting modelled depth compared to single beam testing data between a) 0-35 meters b) 0-15 meters. The red line represents a 1:1 linear line, while the blue is a regression line.

To better mimic the conditions of the ICESat-2 input, the single beam depths between 0-25 meters depth was used as input, resulting in the correlations seen in figure 5.18. Since the ICESat-2 depth around Dhiggaru were ~0-22 meters deep, this resembles the same depth interval. The results are also much closer to what we saw in figure 5.12 for Dhiggaru, with a close to linear correlation between 0-15 meters, and then a poor correlation at deeper depths. With the single beam as training data, the maximum modelled depths are deeper at around 25 meters, compared to the 20 meters when ICESat-2 depths are used for training.

The RMSE and R^2 values are poorer in the 0-15 meter depth interval when single beam depths are used, and it is also clear that the fitted blue line does not lie as close to the red 1:1 line as it did in figure 5.12. The model has a tendency to overestimate the depth, possibly because the single beam training data contains more deep depths (15-25 meters) than the ICESat-2 training data. Therefore the model tries to fit to both shallow and deep data points, resulting in a model that is perhaps slightly better overall, but poorer in the shallow end.

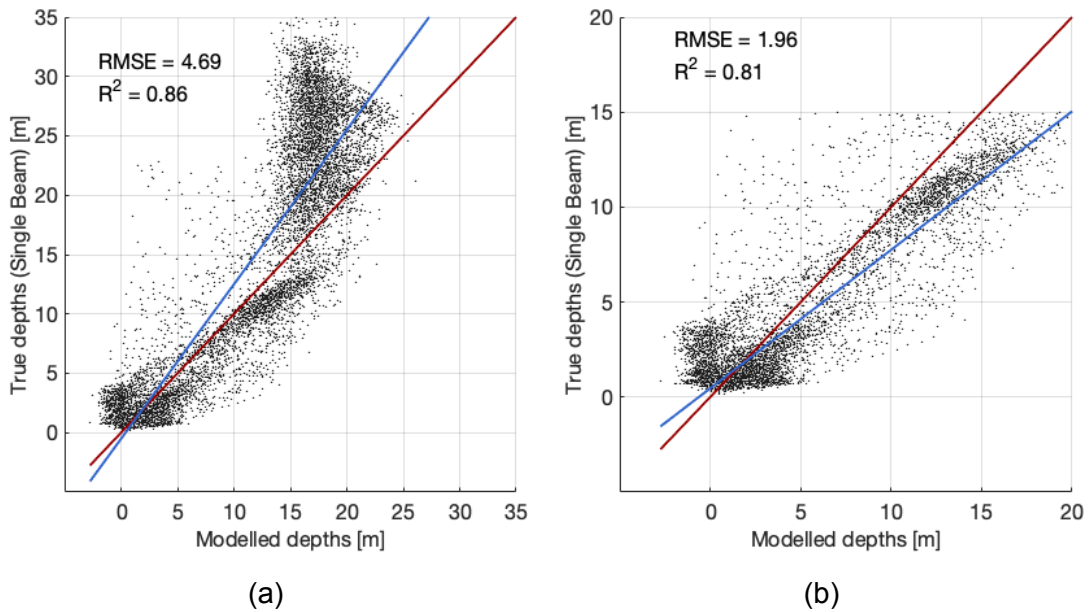


Figure 5.18: Dhiggaru: Single beam depths (0-25 meters) as model input. Resulting modelled depth compared to single beam testing data between a) 0-35 meters b) 0-15 meters. The red line represents a 1:1 linear line, while the blue is a regression line.

It is clear from figures 5.17 and 5.18 that the results are better when the training data is between 0-25 meters than 0-70 meters. This is not surprising, since there is a limit to how deep the optical images can "see". Even on a good day in the clear waters of the Maldives, it is only possible to see the seafloor at 25-30 meters depth. Any area where the depth is greater than this, the water will be optically deep, and have the same reflectance regardless of the depth being 40 or 70 meters. Therefore, it will confuse the model, when it is told that pixels with the same value have different depths.

The correlation in figure 5.17 clearly shows a very poor correlation in the 0-15 meter depth interval. There are also many depths estimated to be above water level, despite single beam having measured the same areas as being 0-5 meters

deep. This problem also occurred with ICESat-2 as model input, however the problem is much worse in the case with single beam training data between 0-70 meters.

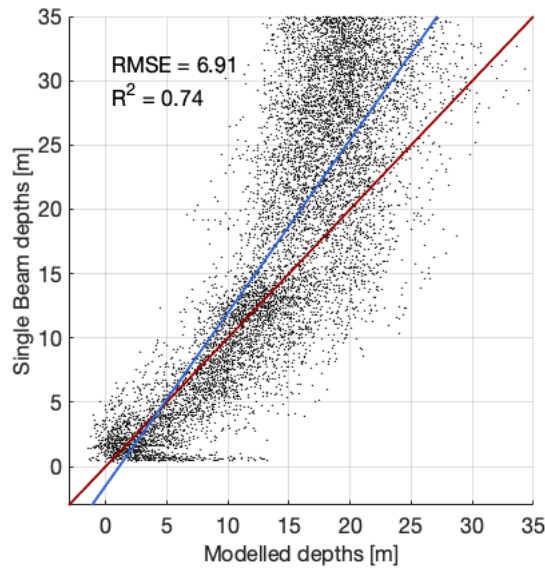


Figure 5.19: Mulah: Single beam depths (0-25 meters) as model input. Resulting modelled depth compared to single beam testing data between 0-35 meters. The red line represents a 1:1 linear line, while the blue is a regression line.

The model was also trained with single beam depths between 0-25 meters for Mulah. The results for Mulah using ICESat-2 depths were very poor, however in figure 5.19 it is clear that the model has successfully estimated the depths between 0-15 meters when using single beam as input. Just like we have seen in the other correlation plots, there is a limit where the correlation is no longer close to the linear red line. However, the correlation in the shallow end is decent, and much better than the result with ICESat-2 as input. This clearly illustrates that ICESat-2 is only useful for training the model, when it is able to estimate a large variety of depths in the area.

6 Conclusion

In this project, two methods for bathymetric mapping were implemented and validated. ICESat-2 LIDAR data was used to estimate seafloor depths along beam tracks as they crossed over three separate islands in the Maldives.

The pre-processing steps for estimating bathymetry from the raw ATL03 data was presented, and the limitations were discussed. The other method for bathymetric mapping combined the ICESat-2 estimated seafloor depths with the multi-spectral properties of Sentinel-2, allowing for surface coverage that ICESat-2 alone could not provide. The Sentinel-2 data from the MSI product also went through several pre-processing steps, before being used for estimating bathymetry. ICESat-2 estimated depths were used as known depths in the linear band model, while selected optical bands from Sentinel-2 were the multi-spectral contribution to the model. The model was implemented as an inverse problem and solved using a least squares regression. This resulted in a fully satellite derived bathymetry.

Both methods were validated using single beam echo sounding data. The validations were carried out with data around three islands in the Maldives: Dhiggaru, Mulah and Buruni. All three islands are surrounded by shallow coral reefs, and the edges of the reefs have very steep slopes into deeper waters. The ICESat-2 estimated bathymetry was found to capture the seafloor well down to 22 and 20 meters for Dhiggaru and Buruni respectively. For these two islands there were RMSE values of 0.77 m and 0.3 m and R^2 values of 0.96 and 0.97. The RMSE for Dhiggaru is higher than for Buruni, however tracks crossing Dhiggaru were more affected by steep slopes that are challenging to capture, and where small displacements in the horizontal coordinates can result in large vertical errors.

These validation results were similar to the ones presented by (Parrish et al., 2019), where the maximum penetration was 0.96 Secchi depth, and the RMSE was 0.43-0.60 m. It is hard to compare directly, since the Secchi depths around the islands are not known precisely, however it is estimated that the maximum penetration around Dhiggaru and Buruni is 0.66-1 Secchi depths.

The third island, Mulah, was more difficult to map. The shallow reef around the island was around 2 meters deep, while the seafloor depths dropped to around 40 meters outside the reef. The seafloor at 40 meters is too deep for the ICESat-2 laser, and therefore most of the estimated depths for Mulah are between 1-2 meters. A visual inspection showed an indication that the seafloor was detected at 30 meters depth, however these data points were indistinguishable from noise,

and they were only discovered because of the single beam validation data. The correlation between the single beam depths and the ICESat-2 estimated depths was good between 1-2 meters, however any depths deeper than 2 meters show a very poor correlation, resulting in an R^2 value of 0.19 between 0-5 m and a RMSE of 1.17 m. The RMSE was 3.5%, 1.5% and 23% of the maximum depths for Dhiggaru, Buruni and Mulah respectively.

The accuracy of the ICESat-2 estimated depths are reasonably good, especially when considering that the single beam depth error is 5-10 cm as well. This means that the measured error between ICESat-2 depths and single beam depths can also be due to errors in the validation data. There is a tendency for ICESat-2 to overestimate the depths compared to the single beam depth measurements. ICESat-2 provides free data from which it is possible to estimate bathymetry with decent accuracy and a revisit time of 91 days makes it possible to track changes in bathymetry over time. However, the data is gathered along three pairs of track beams, that are 3 km apart. This means that ICESat-2 is not able to provide full surface coverage.

By combining ICESat-2 and Sentinel-2 it is possible to use the empirical linear band model method for bathymetric mapping, without the need for in situ measurements. The method is not new, but the need for in situ measurements has its limitations. By using ICESat-2 estimated depths in place of the in situ measurements, it is possible to create a surface covering bathymetric map entirely from free satellite data.

This method was implemented and validated using the single beam data around all three islands. For Dhiggaru and Buruni the best results were between 0-15 meters depth, where the RMSE was 1.38 m and 1.19 m with an R^2 value of 0.86 and 0.83 for the two islands respectively. For Mulah the results were much poorer with a RMSE of 0.95 m and an R^2 value of 0.7 when only looking at depths between 0-5 meters. This resulted in RMSE of 9.2%, 7.9% and 9% of the maximum depth for Dhiggaru, Buruni and Mulah respectively. It was clear from the validation that the model was limited by the ICESat-2 input. For Mulah the correlation between the modelled depths and the single beam depths was only linear between 1-2 meters depth, which is the depth interval where the majority of the ICESat-2 depths were found. For the two other islands the ICESat-2 estimated depths were more evenly distributed, with a decent amount of depth being in the 0-15 meter interval. Therefore the results are much better for these two islands. It was clear when inspecting a residual map of Dhiggaru, that large errors occurred in areas

where the water is most likely optically deep. In these areas the optical images are not able to get reflectance of the seafloor, and therefore not able to correctly estimate the seafloor depths. While the optically deep areas are probably deeper than 15 meters, this appears to be the maximum depth for both Dhiggaru and Buruni, where the depth is modelled correctly.

The validation results were also compared to the study by (Ma et al., 2020), where a similar approach with combining ICESat-2 and Sentinel-2 with the linear band model was used. Their results showed better R^2 values and a similar or slightly worse RMSE than what was found in this project.

To test the limitations of the method, the same model was built but with single beam as known depths instead of ICESat-2 estimate depths. This test made it clear that including depths in optically deep areas only make the model perform worse. When using depths between 0-25 meters, the model performance is similar to when ICESat-2 depths were used as known depths, indicating that having data that covers the entire study area, with more data for training the model is not necessarily an improvement. Therefore, if ICESat-2 is able to estimate depths in the study area, the resulting model appears to be just as good as when using in situ measurements. Sentinel-2 also has a revisit time of only 5 days, making it even easier to track temporal changes in bathymetry. However, the accuracy is not as high as for ICESat-2 on its own, and conventional methods such as echo sounding still have a higher accuracy. The method is limited to areas covered by the ICESat-2 satellite, where a large variety of depths are captured. Murky waters with a small Secchi depth will also be hard to map, as the method is reliant on reflectance of optical light of the seafloor.

Both the ICESat-2 LIDAR bathymetry and the satellite derived bathymetry would be a good supplement for bathymetric mapping. Both methods are cheap with a large spatial coverage (especially the satellite derived bathymetry). They do not have the same penetrating abilities as airborne LIDAR (up to 3 Secchi depths) or multi beam echo sounders (up to 3500 m), however the accuracy of ICESat-2 LIDAR is comparable to these methods. The MAE of ICESat-2 LIDAR bathymetry was 15-30 cm in waters of 0-5 meters depth, while airborne LIDAR has an accuracy of up to 15 cm. The echo sounder methods are still more accurate with a precision of up to 3-5 cm.

7 Future Work

While creating bathymetric maps using ICESat-2 and Sentinel-2 data was successful, there are several things that can be improved in the processing stage and potentially improve the accuracy of the satellite derived bathymetry.

The ICESat-2 data processing could be made more efficient, by creating an automated process for seafloor photon detection. In this project, the method required several manual decisions, and the outlier removal process would in some cases remove potential seafloor photons. The process worked, as a limited number of tracks were processed. An automated process could enable fast processing of many tracks. A process similar to the one used in (Ma et al., 2020) could be implemented, however this method does not successfully remove all the noisy photons either.

By being able to process more ICESat-2 data tracks, it would also make easier to cover larger areas at the time. An entire Sentinel-2 image tile could be processed in one go, using all the ICESat-2 data tracks with valid bathymetry in the 100x100 km area. In this case it would be important to remove optically deep pixels to reduce the data size and computational time. However, it would ensure a large variety of depths that would capture a maximum amount of bottom types. This would also make it possible to create bathymetry maps for an area such as Mulah where the local ICESat-2 bathymetry estimates were insufficient, or areas with no ICESat-2 coverage.

In order to improve the satellite derived bathymetry methods, several ideas could be tested. Since variable bottom types can introduce errors in the model, a classification map of bottom type could be implemented in the linear band model, in an attempt to improve the model. This might also help solve the issue with some areas being estimated as above sea level. It could also be possible to enforce a limit when building the model, where the estimated depth values have to be in a certain interval. It could also be interesting to test the inclusion of more spectral bands, or a band ratio (which is used in the band ratio model (Stumpf et al., 2003)).

Finally, the method should be tested in different water environments. Both in murkier waters, and along reef free coastal areas, where the change from shallow

to deep waters might be less steep and easier to capture. This is needed to gain the full understanding of the method accuracy.

Bibliography

- Abid, D. I. (2020). *Single Beam Echo Sounding Data*. <https://riyan.com.mv/>
- Andersen, O. B. (2015). *DTU15MSS*. <ftp.space.dtu.dk/pub/DTU15/>
- Bramante, J. F., Raju, D. K., & Sin, T. M. (2013). Multispectral derivation of bathymetry in singapore's shallow, turbid waters. *International Journal of Remote Sensing*, 34(6), 2070–2088. <https://doi.org/10.1080/01431161.2012.734934>
- Bundgaard, K. (2020).
- Casal, G., Harris, P., Monteys, X., Hedley, J., Cahalane, C., & McCarthy, T. (2020). Understanding satellite-derived bathymetry using sentinel 2 imagery and spatial prediction models. *GIScience & Remote Sensing*, 57(3), 271–286. <https://doi.org/10.1080/15481603.2019.1685198>
- DMI. (2021). *Nedbør og sol i danmark* [Accessed online on January 10th 2021]. <https://www.dmi.dk/klima/temaforside-klimaet-frem-til-i-dag/nedboer-og-sol-i-danmark/>
- Ernstsen, V., Noormets, R., & Hebbeln, D. (2006). Precision of high-resolution multibeam echo sounding coupled with high-accuracy positioning in a shallow water coastal environment. *Geo-Marine Letters volume*. <https://doi.org/10.1007/s00367-006-0025-3>
- ESA. (2020). *Copernicus Open Access Hub* [Accessed online July-November 2020]. <https://scihub.copernicus.eu/>
- ESA. (2015). *Sentinel-2 User Handbook, 1.2*.
- FAO. (2011). Food and agriculture organization of the united nations: Maldives. *AQUASTAT survey*. http://www.fao.org/nr/water/aquastat/countries_regions/mdv/MDV-CP_eng.pdf
- Gao, J. (2009). Bathymetric mapping by means of remote sensing: Methods, accuracy and limitations. *Progress in Physical Geography: Earth and Environment*, 33(1), 103–116. <https://doi.org/10.1177/0309133309105657>
- Geyman, E. C., & Maloof, A. C. (2019). A simple method for extracting water depth from multispectral satellite imagery in regions of variable bottom type. *Earth and Space Science*, 6(3), 527–537. <https://agupubs.onlinelibrary.wiley.com/doi/abs/10.1029/2018EA000539>
- Hedley, J. D., Harborne, A. R., & Mumby, P. J. (2005). Technical note: Simple and robust removal of sun glint for mapping shallow water benthos. *International Journal of Remote Sensing*, 26(10), 2107–2112. <https://doi.org/10.1080/01431160500034086>

- Irish, J., & White, T. (1998). Coastal engineering applications of high-resolution lidar bathymetry. *Coastal Engineering*, 35(1), 47–71. [https://doi.org/https://doi.org/10.1016/S0378-3839\(98\)00022-2](https://doi.org/https://doi.org/10.1016/S0378-3839(98)00022-2)
- Knaap, M. V. D., Waheed, Z., Shareef, H., & Rasheed, M. (1991). Reef fish resources survey in the maldives. *BAY OF BENGAL PROGRAMME: REEF FISH RESEARCH RESOURCES SURVEY*. <http://www.fao.org/3/a-ae443e.pdf>
- KONGSBERG MARITIME. (2021). Multibeam echo sounder. <https://www.kongsberg.com/globalassets/maritime/km-products/product-documents/em-712-multibeam-echo-sounder>
- Leyendekkers, J. (1977). Prediction of the refractive index of seawater as a function of temperature, pressure, salinity and wavelength. *Marine Chemistry*, 5(1), 29–42. <http://www.sciencedirect.com/science/article/pii/0304420377900135>
- Luthcke, S. B., Pennington, T., Rebold, T., & Thomas, T. (2019). Icesat-2 algorithm theoretical basis document for icesat-2 received photon geolocation (atl03g). *NASA, Version 6*.
- Lyzenga, D., Malinas, N., & Tanis, F. (2006). Multispectral bathymetry using a simple physically based algorithm. *Geoscience and Remote Sensing, IEEE Transactions on*, 44, 2251–2259. <https://doi.org/10.1109/TGRS.2006.872909>
- Ma, Y., Xu, N., Liu, Z., Yang, B., Yang, F., Wang, X. H., & Li, S. (2020). Satellite-derived bathymetry using the icesat-2 lidar and sentinel-2 imagery datasets. *Remote Sensing of Environment*, 250, 112047. <http://www.sciencedirect.com/science/article/pii/S003442572030417X>
- Misra, A., Vojinovic, Z., Ramakrishnan, B., Luijendijk, A., & Ranasinghe, R. (2018). Shallow water bathymetry mapping using support vector machine (svm) technique and multispectral imagery. *International Journal of Remote Sensing*, 39(13), 4431–4450. <https://doi.org/10.1080/01431161.2017.1421796>
- Neumann, T. A., A. Brenner, D. H., Robbins, J., & Saba, J. (2020). Atlas/icesat-2 l2a global geolocated photon data, version 3.
- NOAA. (2014). *National oceanic and atmospheric administration: Field procedures manual* [Accessed online on January 8th 2021]. <https://nauticalcharts.noaa.gov/publications/docs/standards-and-requirements/fpm/2014-fpm-final>
- NSIDC. (n.d.). *ICESat ATL03 Data* [Accessed online July-November 2020]. <https://nsidc.org/data/ATL03/versions/3>
- Overstreet, B. T., & Legleiter, C. J. (2016). Removing sun glint from optical remote sensing images of shallow rivers. *Earth Surface Processes and Landforms*, 42(2), 318–333. <https://onlinelibrary.wiley.com/doi/abs/10.1002/esp.4063>

- Parrish, C. E., Magruder, L. A., Neuenschwander, A. L., & Forfinski-Sarkozi, N. (2019). Validation of icesat-2 atlas bathymetry and analysis of atlas's bathymetric mapping performance. *Remote Sensing*, *11*(1634).
- Quadros, N., Collier, P., & Fraser, C. (2008). Integration of bathymetric and topographic lidar: A preliminary investigation. *Remote Sensing and Spatial Information Sciences*, *37*.
- Quan, X., & Fry, E. S. (1995). Empirical equation for the index of refraction of seawater. *Appl. Opt.*, *34*(18), 3477–3480. <http://ao.osa.org/abstract.cfm?URI=ao-34-18-3477>
- seatemperature.org. (2021). *World sea temperature* [Accessed on January 8th 2021]. <https://www.seatemperature.org/asia/maldives/male-march.htm>
- Stumpf, R. P., Holderied, K., & Sinclair, M. (2003). Determination of water depth with high-resolution satellite imagery over variable bottom types. *Limnology and Oceanography*, *48*(1part2), 547–556. https://aslopubs.onlinelibrary.wiley.com/doi/abs/10.4319/lo.2003.48.1_part_2.0547
- themaldivesexpert.com. (2018). *General information: Mulaku atoll islands (meemu)* [Accessed online on January 10th 2021]. <https://www.themaldivesexpert.com/2657/mulaku-atoll-islands-meemu/>
- University of Salento. (2011). *Ocean salinity* [Accessed on January 8th 2021]. http://phytobioimaging.unisalento.it/StudySites/SitesandSpeciesList/Maldives.aspx?img_folder=Maldives&effect_type=carousel&gallery_width=1000&mode=AD_Gallery#ad-image-0
- U.S. Geological Survey. (2021). *Bathymetric surveys* [Accessed on January 8th 2021]. https://www.usgs.gov/centers/oki-water/science/bathymetric-surveys?qt-science_center_objects=0#qt-science_center_objects
- Vahtmäe, E., & Kutser, T. (2016). Airborne mapping of shallow water bathymetry in the optically complex waters of the Baltic Sea. *Journal of Applied Remote Sensing*, *10*(2), 1–16. <https://doi.org/10.1117/1.JRS.10.025012>
- weatherandclimate.com. (2021). *Average monthly hours of sunshine in malé* [Accessed online on January 10th 2021]. <https://weather-and-climate.com/average-monthly-hours-Sunshine,male-mv,Maldives>
- Wöfl, A.-C., Snaith, H., Amirebrahimi, S., Devey, C. W., Dorschel, B., Ferrini, V., Huvenne, V. A. I., Jakobsson, M., Jencks, J., Johnston, G., Lamarche, G., Mayer, L., Millar, D., Pedersen, T. H., Picard, K., Reitz, A., Schmitt, T., Visbeck, M., Weatherall, P., & Wigley, R. (2019). Seafloor mapping – the challenge of a truly global ocean bathymetry. *Frontiers in Marine Science*, *6*, 283. <https://www.frontiersin.org/article/10.3389/fmars.2019.00283>
- Wozencraft, J. M. (2002). Complete coastal mapping with airborne lidar, *2*, 1194–1198 vol.2. <https://doi.org/10.1109/OCEANS.2002.1192136>

Technical University
of Denmark

Elektrovej, building 327 and 328.
2800 Kgs. Lyngby
Tlf. 4525 1700

www.space.dtu.dk